Chemie der Erde 75 (2015) 403–417

Contents lists available at ScienceDirect

Chemie der Erde

journal homepage: www.elsevier.de/chemer

Geochemistry of trace and rare earth elements during weathering of black shale profiles in Northeast Chongqing, Southwestern China: Their mobilization, redistribution, and fractionation

Sixiang Ling[a], Xiyong Wu[a,b,*], Yong Ren[a], Chunwei Sun[a], Xin Liao[a], Xiaoning Li[a,c], Baolong Zhu[c]

[a] Faculty of Geosciences and Environmental Engineering, Southwest Jiaotong University, Chengdu, Sichuan Province 611756, PR China
[b] Moe Key Laboratory of High-speed Railway Engineering, Southwest Jiaotong University, Chengdu, Sichuan Province 610031, PR China
[c] School of Civil Engineering and Architecture, Southwest University of Science and Technology, Mianyang, Sichuan Province 621010, PR China

ARTICLE INFO

Article history:
Received 23 December 2014
Received in revised form 17 June 2015
Accepted 16 July 2015
Editorial handling - A. Deutsch

Keywords:
Black shale
Trace and rare earth elements
Chemical weathering
Mobilization
Redistribution
REE fractionation

ABSTRACT

In this study, the mobilization, redistribution, and fractionation of trace and rare earth elements (REE) during chemical weathering in mid-ridge (A), near mountaintop (B), and valley (C) profiles (weak, weak to moderate, and moderate to intense chemical weathering stage, respectively), are characterized. Among the trace elements, U and V were depleted in the regolith in all three profiles, Sr, Nb, Ta, Zr, and Hf displayed slight gains or losses, and Th, Rb, Cs, and Sc remained immobile. Mn, Ba, Zn, Cu, and Cr were enriched at the regolith in profiles A and B, but depleted in profile C. Mn, Pb, and Co were also depleted in the saprock and fractured shale zones in profiles A and B and enriched in profile C. REEs were enriched in the regolith and depleted at the saprock zone in profiles A and B and depleted along profile C. Mobility of trace and REEs increased with increasing weathering intensity. Normalized REE patterns based on the parent shale revealed light REE (LREE) enrichment, middle REE (MREE), and heavy REE (HREE) depletion patterns. LREEs were less mobile compared with MREEs and HREEs, and this differentiation increased with increasing weathering degree. Positive Ce anomalies were higher in profile C than in profiles A and B. The Ce fractionated from other REE showed that Ce changed from trivalent to tetravalent (as CeO_2) under oxidizing conditions. Minimal REE fractionation was observed in the saprock zone in profiles A and B. In contrast, more intense weathering in profile C resulted in preferential retention of LREE (especially Ce), leading to considerable LREE/MREE and LREE/HREE fractionation. $(La/Yb)_N$ and $(La/Sm)_N$ ratios displayed maximum values in the saprock zone within low pH values. Findings demonstrate that acidic solutions can mobilize REEs and result in leaching of REEs out of the highly acidic portions of the saprock material and transport downward into fractured shale. The overall behavior of elements in the three profiles suggests that solution pH, as well as the presence of primary and secondary minerals, play important roles in the mobilization and redistribution of trace elements and REEs during black shale chemical weathering.

1. Introduction

Chemical and mechanical weathering leads to the disaggregation of rocks and minerals and the formation of regolith and saprock systems (Aubert et al., 2001). Weathering processes also control the mobilization, redistribution, and fractionation of trace elements and rare earth elements (REEs, La to Lu) in various natural settings. The behavior of trace elements and REEs during chemical weathering has been investigated previously in several protoliths (Nesbitt, 1979; Middelburg et al., 1988; Braun et al., 1993, 2005; van der Weijden and van der Weijden, 1995; Nesbitt and Markovics, 1997; Aiuppa et al., 2000; Panahi et al., 2000; Ji et al., 2004; Brantley et al., 2007; Ma et al., 2007; Ndjigui et al., 2008; Beyala et al., 2009; Feng, 2010, 2011; Gong et al., 2011; Sanematsu et al., 2013; Nguetnkam et al., 2014), including weathering profiles from black shales (Peng et al., 2004; Tuttle et al., 2009; Ma et al., 2011a,b; Jin and Brantley, 2011; Yu et al., 2012). Trace elements and REEs in weathered material can be easily mobilized out of the regolith zone and retained in secondary minerals or colloids in weathering profiles as weathering proceeds (e.g., Sholkovitz, 1992, 1995; Faimon, 2003; Patino et al.,

* Corresponding author at: Faculty of Geosciences and Environmental Engineering, Southwest Jiaotong University, Chengdu 611756, PR China. Fax: +86 028 66367451.
E-mail address: wuxiyong@126.com (X. Wu).

http://dx.doi.org/10.1016/j.chemer.2015.07.004
0009-2819/

2003). Results from prior studies suggest that heavy REEs (HREE) are preferentially transported in solution, while light REEs (LREE) are easily absorbed by oxides/hydroxides or colloids within solid phases. In addition, Ce and Eu anomalies have been found in several weathering profiles within parent bedrocks. These observations provide a record of changes in redox conditions during geological processes (e.g., Brookins, 1989; Ji et al., 2004; Ma et al., 2011b). However, the geochemical behavior of trace elements and REEs during chemical weathering processes cannot easily be generalized due to variations in physico-chemical factors and location-specific weathering environments (Sharma and Rajamani, 2000).

Black shale is a very fine-grained sedimentary rock typically rich in sulfide minerals and organic matter, which contains trace elements (e.g., V, U, Cu, Zn, Mn, Ba, and Pb) (Jaffe et al., 2002; Lipinski et al., 2003; Piper and Calvert, 2009; Anjum et al., 2010). As a result of its sulfide and organic matter content, black shale is especially susceptible to chemical weathering processes, and thus serves to accelerate the decomposition of primary minerals and mobilize trace elements and REEs (Jin et al., 2010; Peng et al., 2007, 2014). Several field and laboratory studies have evaluated the mobility of trace elements in black shale during exposure to acidic groundwater (Lee et al., 1998; Tuttle et al., 2009; Yu et al., 2012) and reported on REE mobility and fractionation (Ma et al., 2011a; Peng et al., 2014). Although these investigations have contributed to the understanding of trace and REEs mobility, the geochemical behavior and factors controlling the mobility of these elements during chemical weathering processes require further investigation.

In this paper, we report on the behavior of select trace elements and REEs in three weathering profiles: mid-ridge (A), near mountaintop (B), and valley floor (C). The study area encompasses the Lower Cambrian black shale in northeastern Chongqing Province, Southwestern China. In this small catchment, profiles A, B, and C are characterized as weak, weak to moderate, and moderate to intense in terms of weathering intensity, respectively (Wu et al., 2015). We compared the composition of weathered products with parent shale in order to develop a better understanding of the geochemistry of trace elements and REEs in black shale profiles at different weathering intensities. The specific objectives of this study were to (i) understand the mobilization and redistribution of trace elements and REEs in weathering profiles during weak to intense chemical weathering; (ii) assess the elemental mobility and REE fractionation under different weathering intensities; (iii) determine inter-element relationships among major elements, trace elements, REEs, and pH in the three profiles; and (iv) identify which factors control the mobility and fractionation of trace elements and REE in black shale weathering profiles.

2. Geographical and geological setting

The study site is an excavated exposure near Chengkou County, northeastern Chongqing Province, China. This site crosses the two first-level tectonic division units of the Qinling orogenic belt and Yangtze Platform (Fig. 1a; Zeng et al., 2012). The Renhe River flows within the catchment from southeast to northwest, eventually joining the Yangtze River through the Han River. Chengkou County has a subtropical climate controlled by East Asian monsoons. The average annual temperature is approximately 13.8 °C and the mean annual precipitation is 1261.4 mm. The V-shaped catchment is characterized by an average local relief of 500 m, and an elevation ranging from 750 m at the riverside to 1250 m at the ridge-top.

The sample site is comprised of a fresh road cut on profiles A, B, and C and surface soil (SS) near the town of Chengkou County (N31°57′–31°58′, E 108°37′–108°39′; Li et al., 2014; Ling et al., 2014). These profiles are covered by Shuijingtuo Formation black shale, Lower Cambrian. The strikes measured on the bedrock at profiles A, B, and C are N53°E, N73°E, and N57°E, and the dips are 60°SE, 78°SE, and 73°SE, respectively (Fig. 1b). The profiles were divided into four zones from surface to bedrock: regolith, saprock, fractured shale, and parent shale (protolith). Wu et al. (2015) reported that profiles A, B, and C possessed a chemical index of alteration (CIA) which ranged from 53.4 to 63.9, 52.4 to 70.8, and 70.6 to 88.7, which indicate weak, weak to moderate, and moderate to intense weathering stages, respectively. Minerals at the site include quartz, muscovite, albite, calcite, dolomite, illite, gypsum, smectite, organic matter, and sulfide (mainly as pyrite) with minor apatite, goethite, kaolinite, and jarosite.

3. Methods

3.1. Analysis techniques

3.1.1. Trace and REE analyses

Samples were collected from each zone for the three profiles, and the sample numbers with corresponding zones and depths are shown in Table 1. After collection, the samples were dried at 65 °C and any plant roots seen in the top 1.5 m in profiles were removed. The samples were ground into 200 mesh (< 75 μm) grains using an agate mortar and pestle prior to laboratory analysis. The processed samples were baked at 700 °C to remove residual organic matter and then digested in a mixed acid solution of HNO_3 + HF in a platinum crucible for trace element and REE analysis. Trace and REEs concentrations were determined using a PerkinElmer Elan 6000 inductively coupled plasma-mass spectrometer (ICP–MS) with elemental detection limits of about 10 ppb for solid samples. The trace and REE concentrations were determined using Rh as an internal during ICP–MS analysis. Analytical precision for trace and REEs was greater than 5% (Liu et al., 1996). Experiments were conducted at the Key Laboratory of Geochronology and Geochemistry, Chinese Academy of Sciences. The analytical results are presented in Tables 1 and 2. Several United States Geological Survey (USGS), Geological Survey of Canada (GSC) and Chinese soils, such as BHVO-2, W-2, GSS-5, GSS-7, SY-4 and GXR-6 (soils) were repeatedly analyzed alongside samples to monitor the quality of ICP-MS measurements, and results were generally within ±10% of the certified values.

3.1.2. pH and SEM-EDS analyses

In order to measure the pH of shale samples, 25 g of deionized water was initially equilibrated with 10 g rock powder in a 50 mL capped Teflon beaker for 20 min. The pH values of the slurry were measured using a calibrated HACH HQ30d acidity meter (USA) with precision better than 0.05. The measurement was repeated on three separate shale samples (Table 2). The handpicked samples were impregnated by vacuum and coated with gold for optical analysis. Scanning electron microscopy (SEM) was used to visualize textures and qualitative energy dispersive spectroscopy (EDS) analysis was performed on select mineral grains to determine phases present. SEM measurements were performed with an Ultra 55 (Car Zeiss Jena) and EDS analysis was conducted using an Oxford IE450X-Max80 at Southwest University of Science and Technology. The SEM was operated at 15 kV with a working distance of 10 mm to provide optimum resolution and minimize charging and sample damage.

3.2. Calculation methodologies

3.2.1. Elemental mobility evaluation method during weathering

To assess the elemental mobility in the weathering profile, concentration (C) of an inert (or conservative) element (i) is commonly compared with the relative loss or gain of a more mobile element (j) by calculating the mass transfer coefficient $\tau_{i,j}$ (e.g., Brimhall and Dietrich, 1987; Brimhall et al., 1991; Anderson et al., 2002;

Table 1
Trace elements content (ppm) at different depth below ground level (bgl, m) in the Chengkou County black shale profile as determined by ICP–MS.

Zonation	depth	Sample	Mn	Rb	Sr	Cs	Ba	Pb	Th	U	Sc	V	Cr	Co	Ni	Cu	Zn	Ga	Ge	Zr	Nb	Hf	Ta	Ti
Regolith	0.10	A-1	1787.40	101.40	135.50	5.72	4829.10	15.98	11.57	20.75	18.02	170.20	89.53	20.46	206.10	62.58	242.50	18.94	1.81	194.40	11.35	5.41	0.90	4969.90
	0.25	A-2	429.00	102.80	124.30	5.66	3982.10	17.82	11.66	17.67	16.65	253.90	97.08	17.05	133.40	44.45	288.20	18.76	1.46	221.40	11.88	5.86	0.94	5274.70
	0.45	A-3	2246.70	106.70	139.40	6.67	3130.00	19.50	12.88	17.54	17.08	226.30	89.39	27.41	143.10	51.02	250.20	19.91	1.73	197.50	11.53	5.50	0.92	5138.00
Saprock	0.55	A-4	2327.30	109.20	143.10	6.86	3186.20	18.93	12.66	17.21	17.73	233.50	88.62	27.78	145.70	52.59	265.10	19.84	1.75	200.70	11.99	5.48	0.93	5271.10
	0.65	A-5	78.99	113.30	95.61	7.65	2421.10	21.32	7.36	13.10	11.62	268.00	109.90	2.32	30.74	16.12	33.59	21.83	1.86	244.50	13.20	6.47	1.01	5818.40
	0.75	A-6	52.74	113.70	104.60	7.31	2441.10	22.17	7.24	14.71	12.14	210.30	105.60	2.34	14.42	17.56	29.58	21.17	1.65	229.00	13.04	5.95	0.99	5657.30
	0.85	A-7	154.50	104.20	236.40	5.58	3971.70	22.70	9.16	14.61	13.36	349.40	103.10	12.67	63.63	32.71	49.86	19.68	1.40	214.00	11.99	5.54	0.94	5340.10
	1.10	A-8	435.00	94.23	658.60	5.12	2978.50	15.13	10.80	16.37	15.26	340.00	92.72	17.51	99.22	42.90	121.00	17.52	1.62	184.50	11.08	4.97	0.87	5016.80
Fractured shale	1.50	A-9	348.70	87.39	654.80	4.78	2432.80	19.37	9.67	21.63	15.64	124.60	82.01	15.95	59.26	44.62	82.35	15.47	1.25	166.20	9.93	4.42	0.77	4767.20
	2.10	A-10	400.30	88.50	862.00	4.55	3339.90	16.07	9.78	24.67	15.28	135.10	72.95	16.74	71.30	41.39	109.20	17.25	1.20	171.80	10.21	4.79	0.79	4859.40
Parent shale	3.00	A-11	405.50	93.55	367.20	4.95	2774.80	25.21	9.94	32.50	16.48	482.80	92.37	17.71	115.50	48.42	97.05	16.29	1.43	166.10	10.53	4.43	0.84	4670.00
Regolith	0.50	B-1	207.40	84.12	300.20	5.98	9785.70	11.41	7.58	9.10	11.51	557.50	402.70	8.16	155.50	172.80	362.70	15.39	2.73	102.00	11.74	2.76	0.84	3541.50
	1.00	B-2	115.40	67.06	641.20	4.66	6280.30	11.10	5.73	12.64	8.37	626.00	526.10	5.46	88.67	218.40	229.40	12.03	2.57	76.62	8.51	1.92	0.62	2486.00
	1.50	B-3	162.40	87.30	573.90	6.13	15261.60	12.41	8.05	14.21	10.39	1379.90	353.10	6.99	89.75	114.00	509.80	14.92	2.87	102.40	11.90	2.69	0.80	3233.90
Saprock	2.00	B-4	564.90	97.78	448.60	5.97	8119.50	23.78	10.32	23.50	13.84	1126.20	192.50	17.78	117.70	96.97	240.60	18.40	2.30	151.50	11.17	3.92	0.86	4355.20
	2.50	B-5	88.40	115.50	448.00	8.40	15136.00	16.67	8.71	27.05	12.90	3839.50	232.40	2.49	185.30	79.80	477.30	18.69	2.59	148.60	10.81	3.72	0.82	3834.40
	3.20	B-6	45.31	104.70	79.68	5.61	4106.20	19.84	10.88	29.75	13.02	1477.10	127.60	9.55	137.20	41.56	125.20	19.26	1.94	212.40	12.04	5.19	0.88	4275.00
	4.00	B-7	239.10	94.92	609.30	5.95	9362.80	18.36	8.91	26.48	11.68	2223.60	154.80	18.34	252.00	80.37	779.20	16.59	1.85	149.60	9.64	3.86	0.76	3764.10
Fractured shale	4.80	B-8	299.10	112.50	339.90	5.76	5150.10	16.60	11.29	29.54	15.58	1339.40	110.20	20.72	193.40	46.95	191.20	19.31	1.84	216.50	11.54	5.26	0.91	4915.90
	5.50	B-9	302.20	117.60	337.10	6.32	4606.00	18.70	11.98	32.32	15.53	1272.60	111.20	22.36	201.70	47.72	212.50	20.81	1.70	220.60	12.18	5.39	0.95	5009.70
	6.20	B-10	292.60	109.40	364.70	5.53	4797.70	17.80	12.02	28.49	14.96	493.70	96.32	19.44	147.50	42.01	132.70	19.47	1.69	212.60	11.99	5.44	0.95	4886.10
Parent shale	7.00	B-11	211.00	79.63	451.40	4.47	3638.70	18.18	7.66	33.16	9.82	1664.90	93.59	17.21	211.60	59.63	373.20	13.42	1.79	125.10	8.00	3.19	0.65	3166.90

Zonation	depth	Sample	Mn	Rb	Sr	Cs	Ba	Pb	Th	U	Sc	V	Cr	Co	Ni	Cu	Zn	Ga	Ge	Zr	Nb	Hf	Ta	Ti
Regolith	0.50	C-1	2052.60	66.83	362.00	3.71	2266.10	19.33	5.05	6.56	14.24	144.00	78.17	21.01	137.00	111.10	180.70	14.89	2.21	133.50	10.32	3.25	0.72	6344.80
	1.00	C-2	196.90	112.80	121.00	6.83	7600.70	25.10	13.26	4.80	15.57	277.90	76.12	2.73	6.00	11.75	26.73	23.20	2.40	188.10	14.20	4.87	1.09	5611.00
	1.50	C-3	93.12	117.60	125.10	7.05	5464.10	36.01	13.60	5.48	15.84	280.90	75.59	1.13	5.80	26.27	21.13	23.17	2.22	185.70	14.01	5.18	1.17	5693.30
Saprock	2.00	C-4	125.40	129.40	112.80	7.72	5193.20	24.14	14.74	4.52	19.79	243.90	85.11	1.32	5.91	27.05	28.17	24.80	2.35	183.80	14.34	4.91	1.12	5688.50
	3.00	C-5	133.50	121.90	108.20	7.56	6122.60	33.06	15.68	4.33	19.97	260.30	84.91	16.95	31.19	143.00	39.29	23.86	2.29	171.60	13.57	4.66	1.07	6328.70
	4.00	C-6	1323.80	115.10	121.60	7.44	6259.70	37.94	13.41	4.73	18.19	243.50	63.12	35.46	66.49	95.26	131.20	22.25	1.88	162.80	12.54	4.42	1.00	4866.90
	5.00	C-7	2644.70	104.20	147.20	6.44	7851.70	44.06	13.32	4.66	17.75	268.90	67.07	34.26	70.02	104.60	163.40	21.46	2.36	154.90	11.95	4.15	0.97	4643.20
	6.20	C-8	2768.10	106.00	150.50	6.50	8252.90	41.53	12.59	4.49	15.14	273.00	75.81	33.81	70.35	101.70	167.40	21.12	2.46	147.70	11.93	3.98	0.92	4626.80
Fracturedshale	8.00	C-9	252.50	110.00	105.50	6.79	4880.70	43.98	13.39	5.84	19.04	323.70	82.74	81.40	105.30	102.00	241.60	21.97	2.03	167.90	12.36	4.51	0.97	5055.40
	9.00	C-10	197.90	82.00	2866.80	5.75	5103.80	12.60	6.39	45.23	9.52	5381.60	1029.50	8.31	116.10	284.30	361.10	14.22	2.79	91.26	8.06	2.35	0.63	2831.00
Parent shale	10.50	C-11	162.40	47.50	2905.10	2.99	3913.60	7.21	4.17	15.85	6.44	373.30	276.80	5.47	54.02	103.90	126.80	8.49	2.33	59.28	7.15	1.45	0.50	2001.80
?	?	C-oxide	136.10	46.13	72.64	4.63	3702.80	15.41	6.61	10.35	13.67	572.50	179.40	34.97	268.10	347.90	781.30	12.88	2.42	336.70	11.92	4.80	0.78	3755.10
Shale chips	0	SS-1	691.80	54.62	208.60	2.57	4104.70	20.17	8.04	12.96	20.74	211.50	107.20	7.46	130.10	139.60	133.20	16.32	1.72	199.40	16.29	4.92	1.33	5950.90
	0	SS-2	295.20	48.84	250.60	2.33	16961.60	19.06	6.60	17.08	14.23	184.40	140.80	9.24	77.57	66.17	52.50	13.89	1.61	168.00	12.27	4.30	0.92	5508.20
	0	SS-3	364.30	78.28	282.60	3.95	1333.50	11.24	10.09	16.64	11.45	106.50	65.18	18.71	52.78	54.75	93.08	14.12	1.33	171.10	9.16	4.23	0.71	3935.00
	0	SS-4	197.20	93.80	369.60	5.01	11418.30	19.53	9.93	36.00	13.17	277.50	93.00	9.27	63.45	33.89	82.85	18.34	1.27	244.50	12.28	6.19	0.97	5201.10

Table 2
The rare earth element contents (ppm) and pH values of bulk samples at different depth (m) in Chengkou County black shale profiles.

Zonation	depth	Sample	La	Ce	Pr	Nd	Sm	Eu	Gd	Tb	Dy	Ho	Er	Tm	Yb	Lu	Y	∑REE[a]	$(La/Yb)_N$	$(La/Sm)_N$	$(Gd/Yb)_N$	$[Ce/Ce^*]_N$	$[Eu/Eu^*]_N$	pH
Regolith	0.10	A-1	34.87	68.41	8.22	33.10	6.89	1.13	6.82	1.10	6.43	1.30	3.60	0.54	3.56	0.52	35.61	176.48	7.03	3.27	1.58	0.99	0.50	6.03
	0.25	A-2	36.22	65.54	8.36	33.27	6.29	1.00	6.31	0.97	6.17	1.28	3.63	0.53	3.55	0.54	41.68	173.67	7.31	3.72	1.47	0.92	0.49	4.25
	0.45	A-3	35.90	69.91	8.09	30.63	5.01	0.74	4.34	0.75	4.71	1.05	3.00	0.46	3.16	0.47	28.68	168.22	8.14	4.63	1.13	1.01	0.48	3.28
Saprock	0.55	A-4	35.70	68.86	7.95	29.87	5.04	0.68	4.30	0.75	4.81	1.05	3.11	0.46	3.13	0.46	29.92	166.16	8.18	4.57	1.14	1.00	0.45	2.82
	0.65	A-5	35.77	61.11	6.97	23.91	3.04	0.34	2.31	0.42	2.79	0.62	1.89	0.30	2.08	0.34	19.14	141.89	12.33	7.59	0.92	0.95	0.39	2.68
	0.75	A-6	36.50	63.05	7.21	24.33	3.03	0.35	2.11	0.37	2.57	0.57	1.70	0.28	1.98	0.31	16.49	144.37	13.24	7.79	0.88	0.95	0.42	3.40
	0.85	A-7	36.30	64.55	8.02	29.22	4.67	0.51	3.87	0.66	4.12	0.89	2.51	0.38	2.58	0.39	26.34	158.66	10.11	5.02	1.24	0.93	0.36	4.24
Fractured shale	1.10	A-8	35.09	65.19	8.40	32.79	6.10	1.00	5.84	0.93	5.45	1.11	3.15	0.47	2.98	0.46	33.51	168.95	8.44	3.71	1.62	0.93	0.51	5.88
	1.50	A-9	29.33	54.14	6.87	27.46	5.34	0.91	5.05	0.83	5.01	1.06	2.97	0.44	2.84	0.43	30.47	142.67	7.42	3.54	1.47	0.94	0.54	6.12
	2.10	A-10	33.01	61.66	7.79	31.01	5.82	1.01	5.66	0.93	5.40	1.10	3.11	0.45	2.97	0.45	31.99	160.36	7.98	3.66	1.58	0.94	0.54	6.88
Parent shale	3.00	A-11	33.96	58.50	7.27	28.48	5.20	0.78	4.99	0.84	4.98	1.08	3.18	0.48	3.21	0.49	31.81	153.43	7.58	4.22	1.29	0.91	0.47	6.52
Regolith	0.50	B-1	38.48	43.99	8.50	32.79	6.51	0.71	7.02	1.07	6.74	1.56	4.44	0.67	4.08	0.63	57.98	157.19	6.77	3.82	1.42	0.60	0.32	7.04
	1.00	B-2	40.05	40.30	9.06	36.14	7.30	1.22	8.95	1.39	8.84	2.08	6.03	0.89	5.30	0.85	83.73	168.40	5.42	3.54	1.40	0.52	0.46	6.55
	1.50	B-3	39.77	48.22	8.69	33.12	6.20	0.44	6.50	1.03	5.99	1.37	3.81	0.56	3.46	0.53	50.17	159.69	8.25	4.14	1.56	0.64	0.21	6.62
Saprock	2.00	B-4	39.38	66.14	9.41	35.84	6.94	0.99	6.48	1.07	6.44	1.41	3.97	0.62	3.86	0.61	43.97	183.16	7.32	3.66	1.39	0.84	0.45	6.20
	2.50	B-5	33.16	48.25	7.73	29.69	5.76	0.19	5.29	0.82	4.78	1.00	2.79	0.45	2.84	0.45	30.71	143.23	8.37	3.72	1.54	0.74	0.11	6.02
	3.20	B-6	32.36	52.38	6.91	23.38	3.84	0.44	3.38	0.67	4.20	0.95	2.84	0.46	3.01	0.47	27.27	135.28	7.72	5.45	0.93	0.86	0.37	4.43
	4.00	B-7	33.22	52.26	7.76	29.99	5.83	0.67	5.68	0.92	5.42	1.18	3.24	0.50	3.04	0.48	37.96	150.19	7.84	3.68	1.55	0.80	0.36	6.50
Fractured shale	4.80	B-8	34.26	63.13	8.26	31.89	6.35	0.99	5.83	0.96	5.56	1.17	3.20	0.52	3.22	0.52	33.67	165.86	7.63	3.48	1.50	0.92	0.50	6.38
	5.50	B-9	37.00	66.52	8.85	33.36	6.46	1.03	5.94	0.97	5.61	1.19	3.35	0.54	3.36	0.54	35.80	174.73	7.89	3.70	1.46	0.90	0.51	6.51
	6.20	B-10	35.85	66.25	8.76	33.36	6.57	1.04	6.20	0.97	5.85	1.21	3.38	0.53	3.38	0.53	35.64	173.86	7.61	3.53	1.52	0.92	0.50	6.80
Parent shale	7.00	B-11	26.48	45.19	6.58	25.04	5.02	0.84	5.00	0.80	4.71	1.06	2.96	0.45	2.78	0.42	33.55	127.34	6.82	3.41	1.48	0.84	0.51	7.12

Zonation	depth	Sample	La	Ce	Pr	Nd	Sm	Eu	Gd	Tb	Dy	Ho	Er	Tm	Yb	Lu	Y	∑REE[a]	$(La/Yb)_N$	$(La/Sm)_N$	$(Gd/Yb)_N$	$[Ce/Ce^*]_N$	$[Eu/Eu^*]_N$	pH
Regolith	0.50	C-1	28.32	47.09	7.25	28.88	6.31	1.38	6.33	1.03	5.69	1.18	3.22	0.47	2.74	0.41	37.54	140.30	7.42	2.90	1.91	0.81	0.67	6.54
	1.00	C-2	49.12	97.35	12.09	44.65	7.53	0.67	4.54	0.84	5.44	1.24	3.54	0.59	3.81	0.61	33.11	232.02	9.26	4.21	0.99	0.98	0.35	6.40
	1.50	C-3	48.57	93.2	11.71	43.84	7.97	1.04	5.59	1.06	6.56	1.42	4.11	0.67	4.45	0.71	35.58	230.89	7.83	3.93	1.04	0.96	0.48	6.16
Saprock	2.00	C-4	47.26	93.63	11.55	42.92	7.91	1.19	6.24	1.08	6.41	1.39	3.92	0.64	4.12	0.66	36.35	228.94	8.23	3.86	1.25	0.98	0.52	6.35
	3.00	C-5	45.47	88.89	11.17	39.71	6.96	0.77	4.24	0.79	5.25	1.13	3.31	0.56	3.64	0.58	29.85	212.46	8.97	4.22	0.96	0.97	0.43	3.85
	4.00	C-6	46.75	91.00	11.46	43.00	8.40	1.16	7.15	1.15	6.76	1.40	3.82	0.63	4.08	0.65	35.56	227.41	8.21	3.59	1.45	0.96	0.46	3.70
	5.00	C-7	45.11	90.02	11.41	42.35	8.47	1.23	7.57	1.27	7.29	1.49	4.08	0.64	4.11	0.66	37.10	225.69	7.87	3.44	1.52	0.97	0.47	4.74
	6.20	C-8	43.56	88.81	10.96	41.58	8.39	1.12	7.42	1.21	6.78	1.37	3.73	0.59	3.63	0.60	34.77	219.74	8.60	3.35	1.69	1.00	0.44	4.65
Fracturedshale	8.00	C-9	41.86	84.7	10.77	41.02	8.11	1.24	6.97	1.17	6.94	1.41	4.07	0.64	4.16	0.65	36.20	213.72	7.21	3.33	1.38	0.98	0.51	6.83
	9.00	C-10	55.55	58.37	13.23	55.40	11.58	2.44	14.81	2.43	15.56	3.67	10.50	1.59	9.27	1.46	137.70	255.85	4.30	3.10	1.32	0.53	0.57	7.22
Parent shale	10.50	C-11	33.29	32.42	7.12	27.78	5.36	1.07	6.24	1.03	6.62	1.57	4.61	0.68	3.99	0.64	66.52	132.42	5.98	4.01	1.29	0.52	0.57	7.26
?	?	C-oxide	24.19	42.13	5.80	21.98	5.30	1.26	8.20	1.36	7.47	1.47	3.87	0.57	3.46	0.52	43.70	127.57	5.02	2.94	1.96	0.87	0.59	6.28
Shale chips	0	SS-1	45.03	69.07	11.19	43.92	9.60	1.87	10.19	1.66	9.80	2.08	5.49	0.78	4.47	0.65	60.97	215.80	7.23	3.03	1.89	0.75	0.58	6.51
	0	SS-2	33.07	50.78	8.59	35.64	8.41	0.81	8.29	1.28	7.14	1.46	3.84	0.56	3.21	0.48	42.52	163.54	7.40	2.54	2.14	0.74	0.30	6.88
	0	SS-3	26.86	52.27	6.97	27.86	6.23	1.20	5.42	0.88	4.72	0.96	2.61	0.40	2.57	0.39	26.38	139.32	7.51	2.78	1.75	0.94	0.63	6.83
	0	SS-4	36.19	66.19	8.22	28.70	5.01	0.11	4.31	0.75	4.45	0.95	2.76	0.44	2.85	0.45	27.70	161.36	9.11	4.66	1.25	0.94	0.07	6.79

[a] ∑REE = the sum of La~Lu, $[Ce/Ce^*]N(p) = CeN(P)/(LaN(P) \times PrN(P))0.5$, $[Eu/Eu^*]N(P) = EuN(P)/(SmN(P) \times GdN(P))0.5$, and (La/Yb)N, (La/Sm)N, (Gd/Yb)N, where the subscript N implies chondrite-normalized value (see Sun and McDonough, 1989) and P indicates normalization by parent shale in each profile.

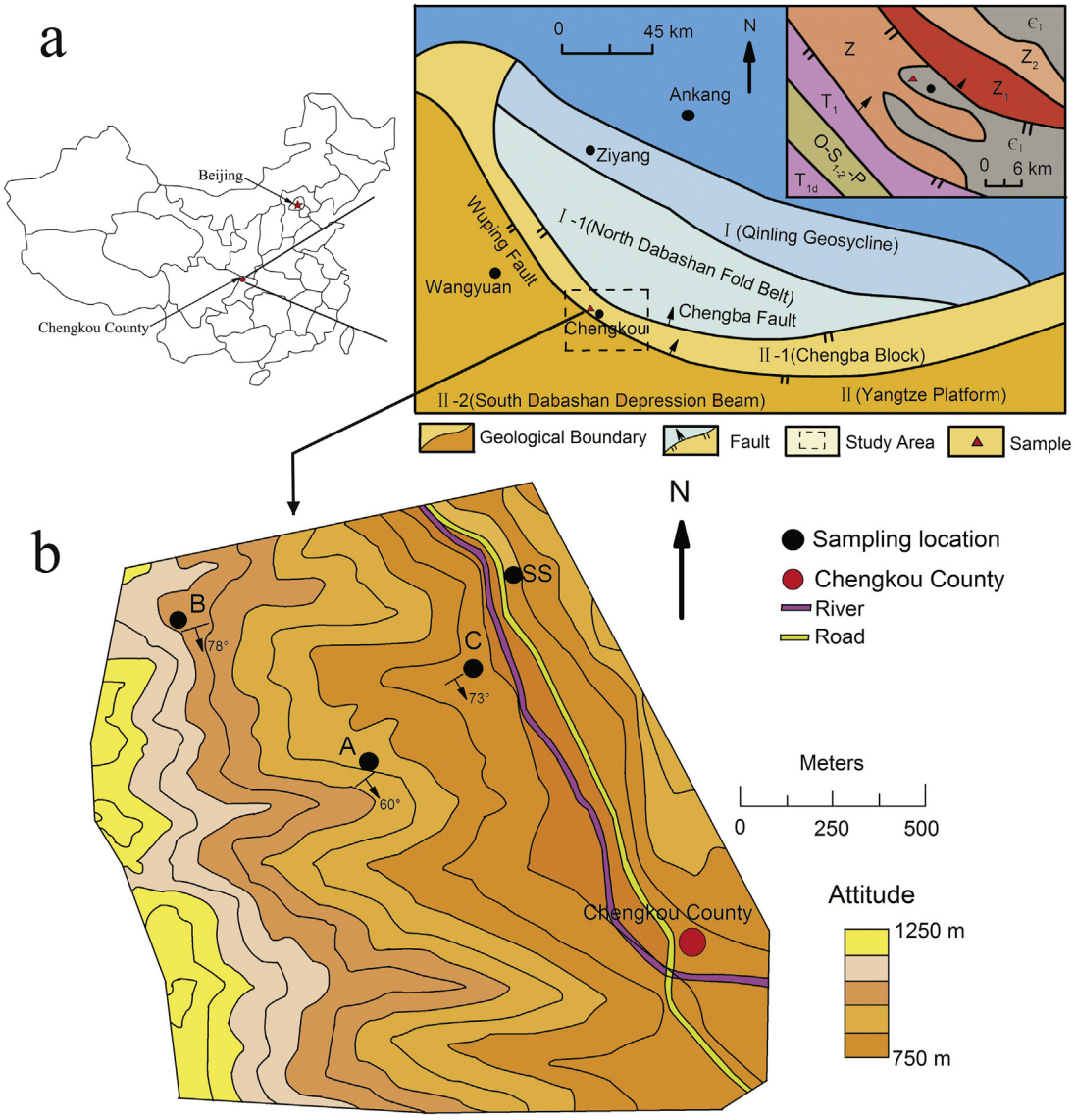

Fig. 1. (a) Geological structure diagram of Chengkou County; (b) Sampling site of Shuijingtuo Formation black shale, Lower Cambrian, at Chengkou County. The samples were colltected from nearby moutaintop (B), midridge (A), valley floor (C), and Surface Soil (SS), respectively.

Amundson, 2004; Tuttle et al., 2009; Ma et al., 2011a). The value of $\tau_{i,j}$ can be calculated by:

$$\tau_{i,j} = \frac{C_{j,w}}{C_{j,p}} \times \frac{C_{i,p}}{C_{i,w}} - 1 \quad (1)$$

where, $C_{j,w}$ and $C_{j,p}$ are the concentrations of phase j in weathered and protolith materials, respectively; $C_{i,w}$ and $C_{i,p}$ are the concentrations of the inert (conservative) index phase (Ti in this instance; Ling et al., 2014) in weathered and protolith materials. In this study, we chose the bottom sample of each profile, indicated as protolith shale (A-11, B-11, and C-11). Positive $\tau_{i,j}$ values indicate external additions of element j, negative $\tau_{i,j}$ values show depletion, and zero values suggest that element j is immobile in the weathered material (w). The results of mobilization of trace elements and REEs for each profile are presented at Appendix Table 1 of Supplementary information.

3.2.2. Statistical analysis

The inter-element relationships among major elements, pH, organic matter content, and trace element and REE content were evaluated through correlation analysis. The Pearson correlation coefficient (r) measures the strength of linear relationships between two quantitative variables and helps to reveal differences among variables relevant to chemical weathering processes. The significance of linear correlations was determined using the Pearson product-moment correlation coefficient with SPSS version 19. This method allows for statistical evaluation of analytical results and identification of potential relationships between elements and other test values. The statistical results for each profile are presented at Appendix Table 2 of Supplementary information.

4. Results

4.1. Distribution of trace and rare earth elements

4.1.1. Distribution of trace elements and variation with depth

The results of the trace element analysis are summarized in Table 1. Three groups of trace elements can be identified based on their behavior along the black shale profiles:

(1) Large ion lithophile elements (LILE), including Mn, Rb, Ba, Sr, Pb, Cs, Th, and U (Schilling, 1973). In profile A, Rb and Ba were observed higher concentrations in the weathered shale than in parent shale, whereas Sr, Pb, and U decreased considerably in the weathered shale (Table 1). The Mn concentration gradually decreased from the bottom of the profile upward to a depth of 0.75 m and then sharply increased at depths above 0.75 m, whereas concentrations of Cs and Th were not strongly depth-dependent. In profile B, Rb and Ba were enriched in weathered shale relative to the parent shale, while Pb and U decreased along this transect. Concentrations of Mn and Sr were highly variable with depth with minimum values of 45.31 ppm and 79.68 ppm, respectively, measured at a depth of 3.2 m. In profile B, Cs and Th followed trends similar to those observed in profile A. In profile C, comparisons between parent shale and weathered shale showed that concentrations of Rb, Cs, Pb, and Th increased, whereas Sr and U decreased with decreasing depth. Mn was concentrated in the lower regions of saprock and at the top of the regolith, with minimum concentrations measured at a depth of 1.5 m. In profile C, Ba concentrations fluctuated along this transect and with a maximum concentration of 8252.90 ppm measured in the saprock zone at a depth of 6.2 m.

(2) Trans-transition elements (TRTE), including Co, Cr, Cu, Ni, V, Sc, and Zn (Jenner, 1996). Concentrations of Sc generally had less variation compared with other TRTEs along the three different transects (Table 1). In profile A, V concentrations were considerably lower compared to the parent shale, and Co, Ni, Cu, and Zn decreased from the protolith to the middle part of the saprock (minimum value observed at 0.65–0.75 m) and then sharply increased above 0.65 m in depth. Conversely, Cr was concentrated in the middle part of the saprock and decreased above 0.55 m in depth. In profile B, Cr was observed at relatively high concentrations, while Ni and Co were found at relatively low concentrations in weathered shale compared with parent shale. V concentrations were fairly low in weathering products compared with parent shale. Concentrations of Cu and Zn fluctuated with depth and were highest in the regolith and saprock zone, respectively. In profile C, V and Cr decreased from the protolith to regolith, except for samples C-10 at a depth of 9.0 m. Cu concentrations were fairly constant from 3.0 to 10.5 m in depth, but sharply decreased at 1.0–2.0 m. Concentrations of Co, Ni, and Zn in the protolith were lower than levels observed at depths of 4.0–9.0 m, but greater than those measured above 4.0 m, except for sample C-1 at 0.5 m depth.

(3) High-field strength elements (HFSE), including Ga, Ge, Zr, Nb, Hf, Ta, and Ti (Saunders et al., 1980; Panahi et al., 2000). Comparison of parent shale and weathered shale showed that concentrations of Ge and Ta remained relatively constant along three profiles, whereas Ga, Zr, Hf and Ti increased (except for Zr and Hf element in the regolith zone in profile B). Nb concentration remained relatively constant in profile A, but was present at higher levels in weathered products than in protolith in profile B and C.

4.1.2. Total REE + Y contents and variation with depth

REE concentrations within the three profiles and SS are shown in Table 2, and the average REE concentrations of each zone are provided in Fig. 2. In this paper, we divided REE (La to Lu) into light REE (LREE, La to Nd), middle REE (MREE, Sm to Dy), and heavy REE (HREE, Ho to Lu). Concentrations of total REEs ranged from 141.89 ppm to 176.48 ppm, 127.34 ppm to 183.16 ppm, and 127.57 ppm to 255.85 ppm in profiles A, B, and C, respectively (Table 2). In profile A (Fig. 2a), the total average LREE content gradually increased from parent shale upward to the regolith zone. The total average MREE, HREE and Y contents diminished from the parent shale to saprock zone, and increased at the regolith zone. In profile B (Fig. 2b), the average LREE content was enriched in weathered shale compared with the parent shale, but displayed a maximum average value in fractured shale (142.50 ppm). The average MREE and HREE contents ranged from 16.37–23.30 ppm and 7.67–12.09 ppm, respectively, with maximum values for both occurring in the regolith zone. Y content increased sharply from the parent shale to regolith material. In profile C (Fig. 2c), the average LREE content was enriched in the weathered products (ca. 1.7- to 1.9-fold higher than in the parent shale). The average MREE content increased in fractured shale (32.05 ppm), but decreased sharply in the saprock and regolith. The HREE and Y displayed similar patterns to those observed with MREE, in that the contents of HREE and Y increased from the parent to fractured shale, but decreased in the saprock and regolith zone (Fig. 2c). In addition, the average LREE content at SS was determined to be 137.63 ppm, considerably lower compared with the regolith of profile C. MREE, HREE, and Y contents were 23.03, 9.34, and 39.39 ppm, respectively (Table 2), levels approximately equal to those measured in the regolith material of profile C.

4.2. Mobilization of trace elements and REE + Y during weathering

4.2.1. Mobilization of trace elements during weathering

The gain or loss of trace elements calculated using Eq. (1) is shown in Fig. 3. The $\tau_{Ti,j}$ values for Rb, Th, and Sc approached zero in all three profiles, indicating that these elements were relatively immobile along the three transects, except for Th and Sc, which displayed slight losses in the saprock in profile A (Fig. 3a and b). The $\tau_{Ti,j}$ values for Pb were less than zero in profiles A and B (Fig. 3a and d) and considerably greater than zero throughout profile C (Fig. 3g). The $\tau_{Ti,j}$ pattern for Ge displayed enrichment in the regolith and upper part of saprock zones and depletion in the lower part of saprock and fractured shale zones in profiles A and B, showing an "addition" pattern (Fig. 3c and f; Brantley et al., 2007). The $\tau_{Ti,j}$ values of U and V were less than zero in all three profiles (except for V at 2.5 m in profile B) and tended to decrease with decreasing depth ("depletion" pattern).

In profile A, the $\tau_{Ti,j}$ values of Sr were less than zero in regolith and saprock zone, but greater than zero at the bottom of saprock and fractured shale. Conversely, the $\tau_{Ti,j}$ values for Mn, Ba, Co, Ni, Cu, and Zn were greater than zero in the regolith, less than zero in the middle part of the saprock zone, and close to zero in the fractured shale (Fig. 3a and b). The $\tau_{Ti,j}$ values for Cs were near zero in the regolith and fractured shale, but showed $\tau_{Ti,j}$ values greater than zero in the saprock zone (Fig. 3a). The $\tau_{Ti,j}$ values for Nb, Ta, and Cr approached zero, but Zr, Hf, and Ga displayed similar $\tau_{Ti,j}$ patterns, with $\tau_{Ti,j}$ values decreasing slightly with depth in profile A (Fig. 3b and c).

In profile B, the $\tau_{Ti,j}$ values for Cs, Ba, Sr, Cu, and Cr were considerably greater than zero in the regolith and saprock zones, with maximum values observed in the regolith (3.11 for Ba, 0.81 for Sr, 6.16 for Cr, and 3.67 for Cu) and in the saprock (0.55 for Cs), in agreement with an "addition" pattern (Fig. 3d and e). The $\tau_{Ti,j}$ values for Mn peaked at the top of the saprock zone (maximum value of 0.95), but less than zero in the remainder depths (Fig. 3d). For Ni, Co, and Zn, $\tau_{Ti,j}$ values were less than zero in the regolith and upper part of the saprock zones, but a peak value was observed at the bottom of saprock zone (4.0 m) (Fig. 3e). Nb, Ta, and Ga accumulated along this transect and displayed an *"addition"* pattern (Fig. 3f). By contrast, Zr and Hf were depleted in the regolith zone and enriched within the middle part of the saprock at a depth of 3.2 m (0.26 for Zr and 0.21 for Hf) (Fig. 3f).

In profile C, $\tau_{i,j}$ values of trace elements (except for Mn, Pb, and Co) became increasingly negative with decreasing depth (Fig. 3g–i). The $\tau_{Ti,j}$ values for Mn and Co were greater than zero at deeper parts of the profile (except for C-1) and less than zero in the remainder of the regolith and the upper part of saprock zones. For Cs, Ba, Sr, Cr, Ni, Cu, Zn, Ge, Nb, and Ta, $\tau_{Ti,j}$ values were significantly less than zero throughout the profile C, indicative of high mobility and "depletion"

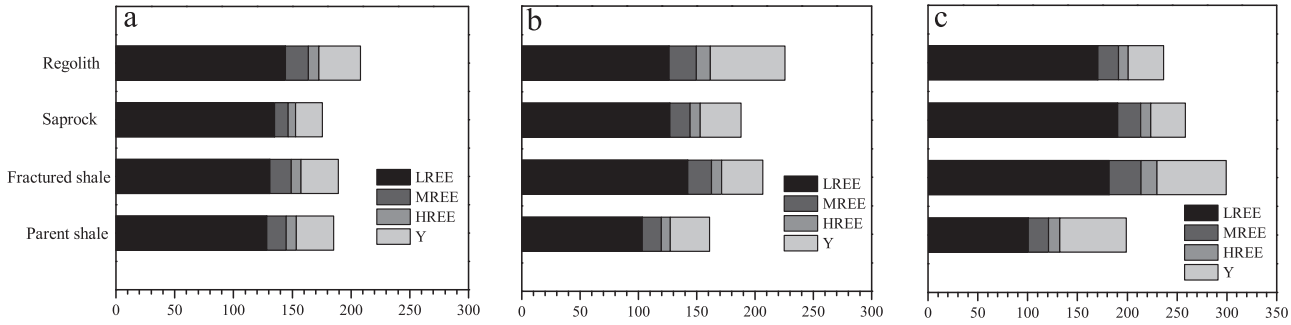

Fig. 2. Total average contents of LREE, MREE, HREE and Y of each weathering zone in (a) profile A, (b) profile B, and (c) profile C at Chengkou County.

patterns (Fig. 3g–i). The $\tau_{i,j}$ values for Zr, Hf, and Ga were greater than zero (except for sample C-1), showing an "addition" pattern (Fig. 3i).

4.2.2. Mobilization and redistribution of REE + Y during weathering

Using Eq. (1), the $\tau_{i,j}$ values of REEs and Y are provided in Fig. 4. In profile A, all REEs showed similar variation patterns. The REEs accumulated at low levels in the regolith, but were considerably depleted in the saprock zone (Fig. 4a–c). Based on estimates from the $\tau_{i,j}$ values calculated for REEs, accumulation in the regolith reached maximum values of 0.10 for LREE, 0.36 for MREE, and 0.13 for HREE + Y. Conversely, MREE was depleted in the saprock (maximum of −0.65 for Eu and Gd), followed by HREE (−0.56 for Ho), and LREE (−0.33 for Nd). REEs mobility patterns in profile A can be considered as "biogenic" with "immobile" multiple patterns.

In profile B, all REEs displayed similar patterns (excluding Ce) and similar behavior to the patterns observed in profile A (Fig. 4d–f). All REEs (excluding Ce) were enriched in the regolith zone. A peak $\tau_{i,j}$ value was measured at a depth of 1 m (sample B-2) and $\tau_{i,j}$ values were observed to increase with increasing atomic number. All REEs (excluding Ce) were slightly depleted in the saprock and fractured shale. The losses observed in MREEs (minimum −0.50 for Gd, −0.81 for Eu) were greater than those of HREEs (−0.34 for Ho), followed by LREE (−0.31 for Nd) in the saprock zone. Ce was separated from other REEs and remained immobile along this transect (except for B-1). Y exhibited a pattern similar to that of HREE and was clearly enriched within the regolith and depleted in the saprock and fractured shale zones (Fig. 4f). All REEs patterns in profile B can be regarded as "addition" patterns.

In profile C, REEs (excluding Ce) showed similar variation patterns (Fig. 4g–i). The REEs were largely depleted from the regolith, saprock, and upper portion of fractured shale zones, but enriched at the bottom of the fractured shale. Ce displayed a constant enrichment pattern along this transect, except for sample C-1 (Fig. 4g). The $\tau_{i,j}$ value for Y was less than zero and tended to decrease with decreasing depth. All REE patterns of profile C are suggestive of "depletion" patterns.

4.3. REE normalization

REE patterns normalized to the parent shale are shown in Fig. 5. In profile A, the LREEs concentrations are concentrated parallel and close to the parent shale. MREE- and HREE-depleted patterns were observed in the saprock zone (Fig. 5a). However, MREEs and HREEs in the regolith material displayed normalized ratios above 1 with more enrichment observed for MREEs than for HREEs. In profile B, normalization of samples to the parent shale showed that most samples with ratios above 1 exhibited REE-enriched patterns, whereas samples (e.g., B-6) in the saprock zone were generally MREE-depleted, especially Eu (Fig. 5b). In profile C, the samples (except for C-oxide) normalized to the parent shale exhibited LREE-enriched patterns, with greater enrichment observed for Ce than for other LREEs (Fig. 5c). The MREE patterns were enriched along the fractured shale and the lower portion of saprock zone relative to parent shale, whereas the regolith and upper portion of the saprock zones displayed a MREE-depleted pattern (excluding Sm), especially for sample C-2 and C-5. HREE patterns, however, were distinctly depleted in profile C (Fig. 5c).

4.4. Ce and Eu anomalies

Ce has been shown to be redox-sensitive under weathering conditions; it can be oxidized to the tetravalent state and is widely used as an indicator of redox conditions (e.g., Taylor and McLennan, 1995; Morgan et al., 2012; Sanematsu et al., 2013). Thus, oxidizing conditions generally result in precipitation with Ce enrichment forming positive Ce anomalies (German et al., 1991; Alibo and Nozaki, 1999), while reducing conditions are associated with negative Ce anomalies. The ratios of $[Ce/Ce^*]_{N(P)}$ are plotted in Fig. 6 for the three profiles. The $[Ce/Ce^*]_N$ ratio of parent shale was 0.91, 0.84, and 0.52 in profile A, B, and C, respectively (Table 2). Therefore, $[Ce/Ce^*]_N$ ratios displayed negative anomalies in all profiles, indicating that black shale was deposited under reducing conditions. The $[Ce/Ce^*]_P$ ratio was slightly greater than 1 in profile A (Fig. 6a), indicating that Ce was gradually oxidized and precipitated as CeO_2 in oxidized environment. In profile B (Fig. 6b), the $[Ce/Ce^*]_P$ anomaly became negative in the regolith zone (Ce concentration is less than that in the parent shale), indicating that Ce depletion occurs more readily in this zone relative to other REEs. The $[Ce/Ce^*]_P$ ratios for remaining samples were near 1, indicating that under oxidized environment. In contrast, the $[Ce/Ce^*]_P$ value of samples in profile C exhibited significant positive Ce anomalies (Fig. 6c). It can be concluded that $[Ce/Ce^*]_P$ values generally exhibited positive anomalies in the three profiles, indicating that Ce (III) oxidized to Ce (IV) as insoluble CeO_2 and that an oxidizing environment was present during weathering processes.

The ratios of $[Eu/Eu^*]_{N(p)}$ are plotted in Fig. 6. All samples in the three profiles showed significant negative $[Eu/Eu^*]_N$ anomalies. Theoretically, Eu is oxidized to trivalent in oxidizing environments and reduced to divalent in reducing environments (Brookins, 1989; MacRae et al., 1992). In profile A (Fig. 6a), most of $[Eu/Eu^*]_P$ ratios were greater than 1. These positive $[Eu/Eu^*]_P$ anomalies suggest that profile A was transformed into oxidizing environment during weathering. In profiles B and C (Fig. 6b and c), the $[Eu/Eu^*]_P$ ratios calculated for weathered samples revealed negative anomalies (excluding sample C-1) along the transects. Previous studies have suggested that Eu is preferentially mobile and released from rocks under reducing conditions during water-rock interaction (Sverjensky, 1984; Bau, 1991). Therefore, the Eu may have

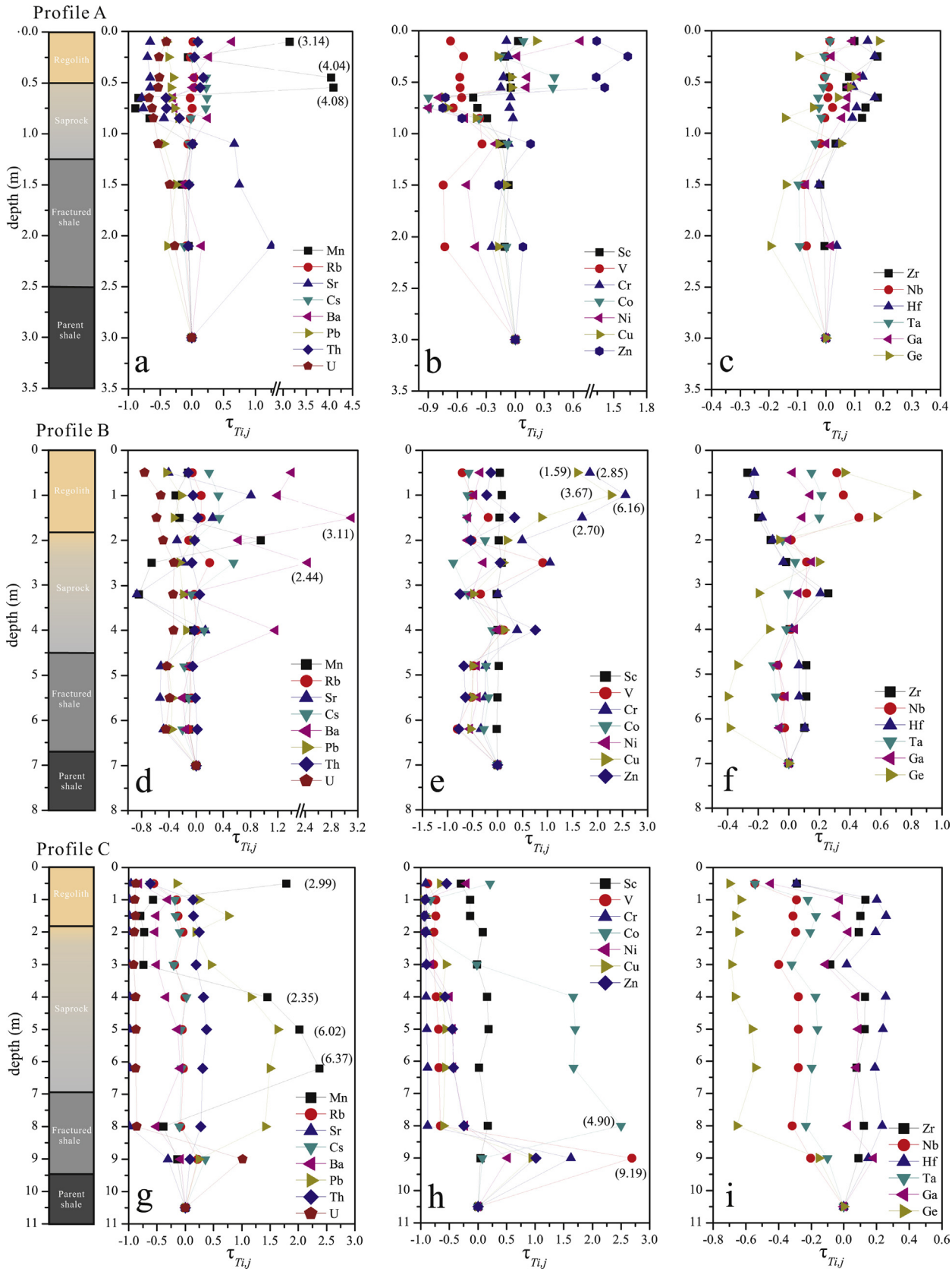

Fig. 3. The mass transfer coefficients ($\tau_{Ti,j}$) for trace elements in profiles A (a–c), B (d–f) and C (g–i) at Chengkou County.

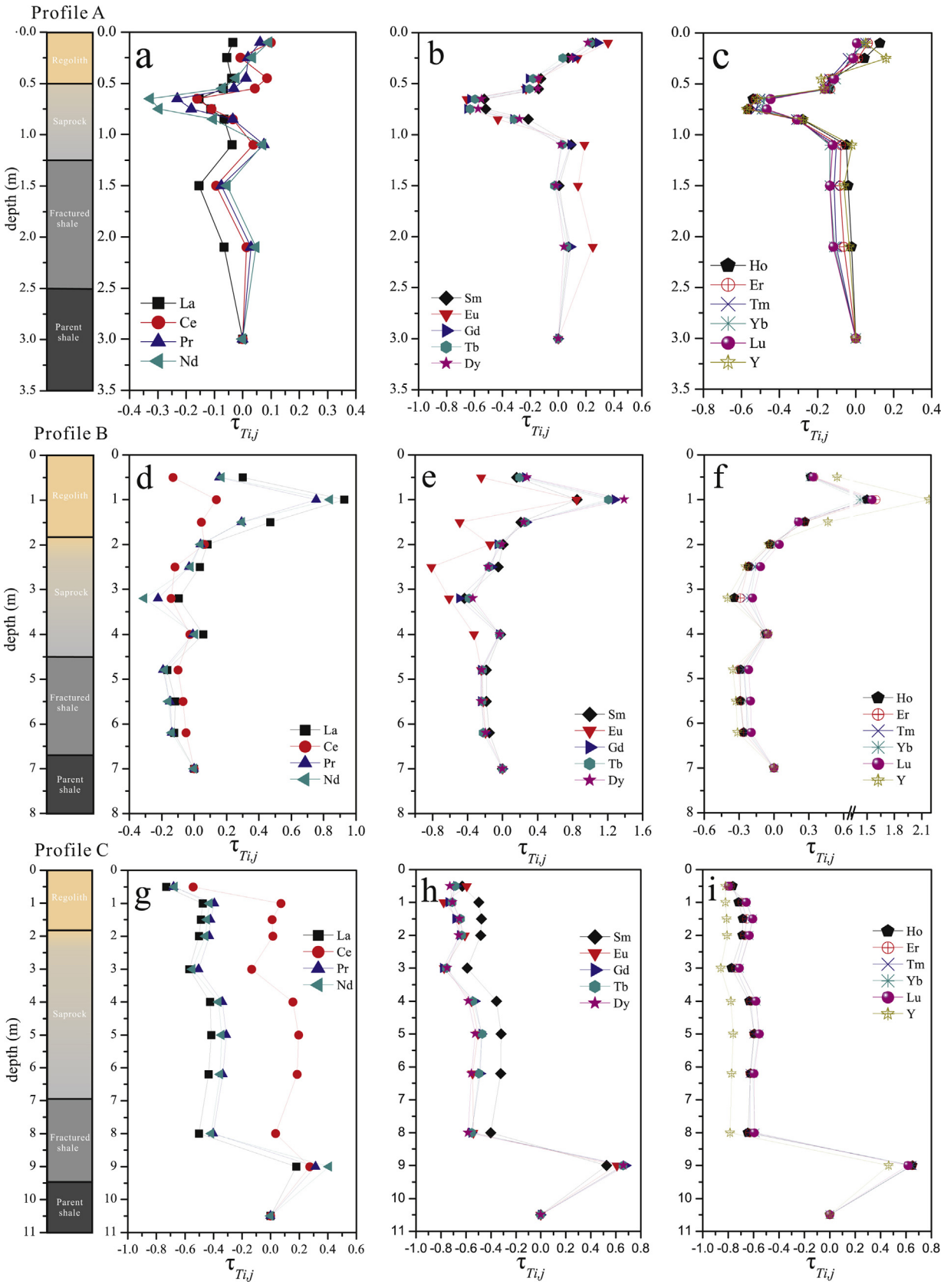

Fig. 4. The mass transfer coefficient (τ) for LREE (a, d, g), MREE (b, e, h), and HREE + Y (c, f, i) in profiles A (a–c), B (d–f), and C (g–i) at Chengkou County.

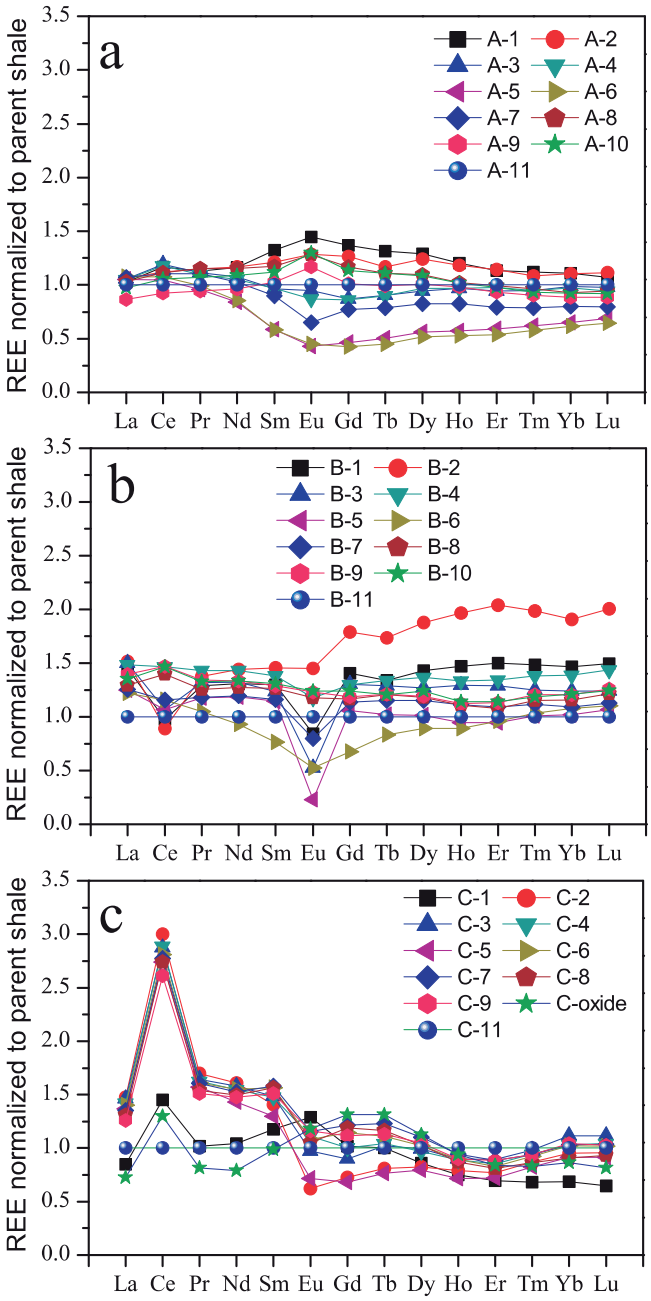

Fig. 5. REE patterns normalized to parent shale in three profiles. Samples from (a) profile A, (b) profile B, and (c) profile C (excluding sample C-10).

been preferentially removed from other REEs, resulting in native $[Eu/Eu^*]_P$ anomalies when the weathering degree reached a moderate to intense stage.

4.5. SEM-EDS

Specimens analyzed from C-8 in the saprock zone displayed distinct crystal and sheet structures (Fig. 7a). The block-like crystal in Fig. 7a yielded Ca, P and F signals, suggesting an apatite mineral containing Ni, Nb, and Ta (Fig. 7c). Fine grain and tiny spheroids were observed to cover the surface of sample C-3 from the regolith zone (Fig. 7b) with grain sizes less than 0.5 μm in diameter. EDS measurements of select spheroid material yielded with K, Fe, Al, and Si signals, indicative of Fe/Al-oxide or hydroxide minerals rich in La, Ce, Pr, Nd, Sm, and Ho (Fig. 7d).

5. Discussion

5.1. Behavior and specific relationship of trace elements during weathering

5.1.1. Behavior of LILE

The LILE are known to be highly soluble and susceptible to chemical weathering processes, with Mn, Sr, and Ba considered the most easily mobilized elements (Fig. 3a, d and g). Inconsiderable enrichment of Mn was persisted in the top section of profiles A and C, where enrichment may result from input sources such as atmo-

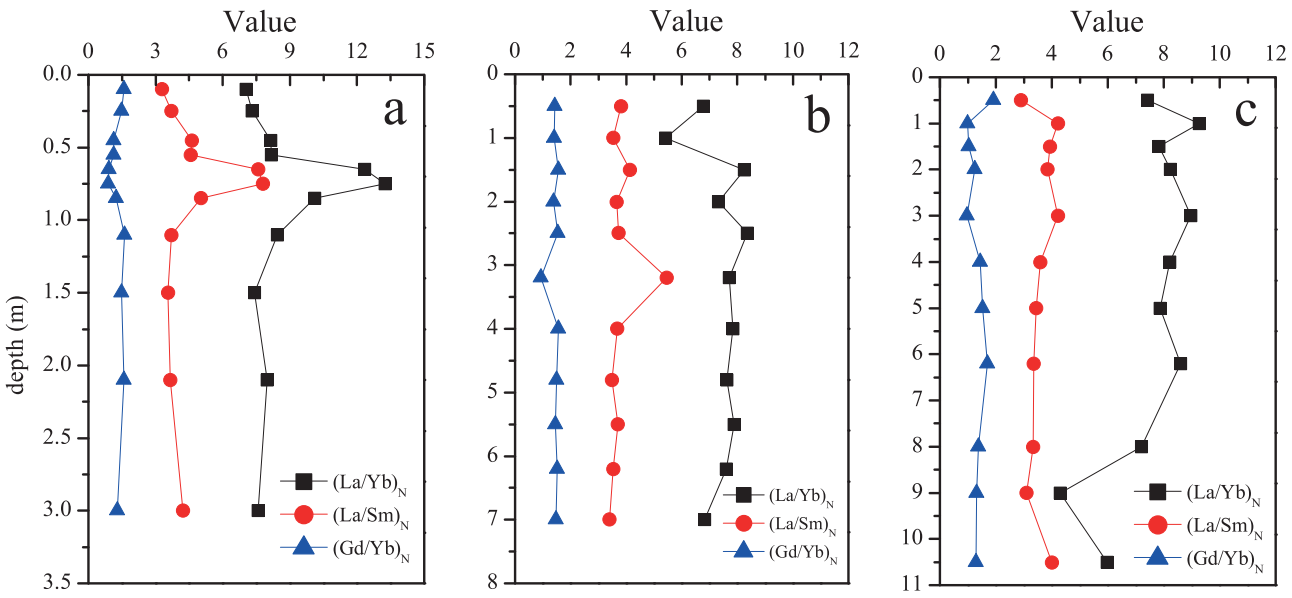

Fig. 6. Depth profiles showing variations in Ce and Eu anomalies in (a) profiles A, (b) profile B, and (c) profile C at Chengkou County.

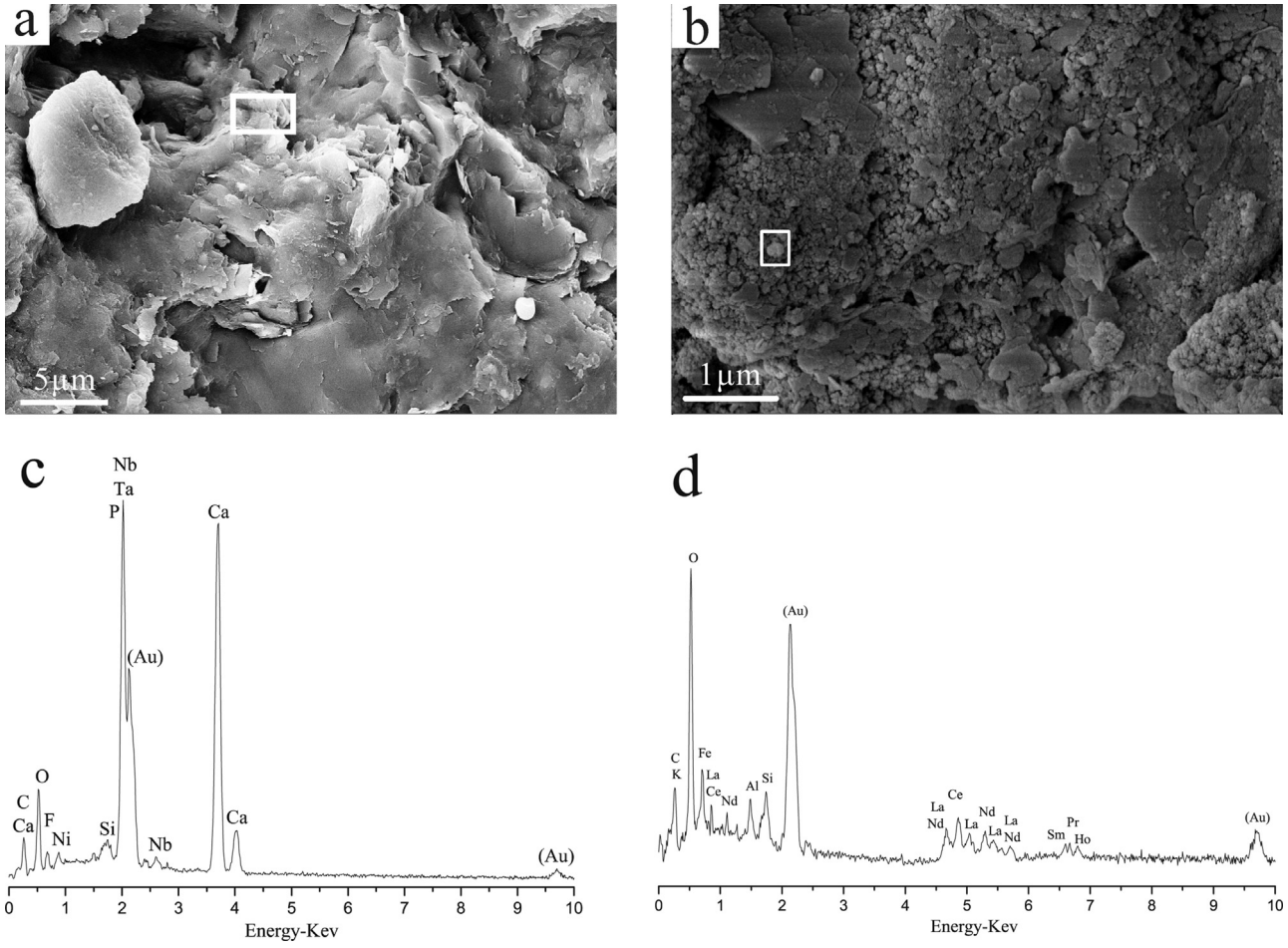

Fig. 7. (a) SEM photomicrographs with EDS analysis of apatite (sample C-8) from profile C; (b) SEM micrographs of spherical aggregates of Fe/Al-oxides or hydroxides on surface of silicate (sample C-3) from profile C; (c) and (d) EDS analysis was focused from white box in (a) and (b), respectively. Au peak was from gold powder sputter-coated onto sample.

spheric contamination, vegetation, or other sources (Herndon et al., 2011). Manganese (II) is also known to leach from host minerals and transfer through aqueous solutions. However, when it is oxidized into Mn (III, IV), Mn can subsequently precipitate as insoluble Mn-oxide or hydroxide in the weathering profile (e.g., Koppi et al., 1996). Therefore, Mn was likely removed from the middle part of the saprock zone in profiles A and B as a result of exposure to acidic solutions (Fig. 3a and d), and re-precipitated in deep sections of profile C (Fig. 3g). The mobility patterns for Rb and Cs were frequently co-associated with K, because they had significant positive relationship with each other in profiles A, B, and C ($r_{K\text{-}Rb}$ = 0.962, 0.943, 0.741; $r_{K\text{-}Cs}$ = 0.872, 0.413, 0.650; $r_{Rb\text{-}Cs}$ = 0.954, 0.621, 0.981). Sr is controlled by host mineral because it is hosted in Ca-bearing minerals and co-association mobilized with Ca during weathering ($r_{Ca\text{-}Sr}$ = 0.983, 0.469, 0.859).

U displayed depletion pattern during weathering process. This observation was attributed to weathering of U-bearing mineral under oxidizing conditions which resulted in the dissolution and removal of U from the profile through oxidation of U^{4+} to highly soluble U^{6+} (e.g., Panahi et al., 2000). Uranium (VI) was adsorbed onto Fe-oxide minerals (e.g., goethite) and the co-precipitation occurred in the saprock (Moyes et al., 2000; Duff et al., 2002). The correlation coefficient demonstrates that U is likely associated with Fe_2O_3 in profiles A and B ($r_{Fe\text{-}U}$ = 0.594, 0.401). However, U is not strongly correlated with Fe_2O_3 in profile C ($r_{Fe\text{-}U}$ = −0.192), where U may transform into oxic phases as very soluble UO_2^{2+}. These results suggest that an intense weathering which leads to the formation of an oxic environment may not alone result in U enrichment. Th mainly exists in black shale as $ThSiO_4$ and ThO_2, with variable but generally high resistance to weathering (Braun et al., 1993).

5.1.2. Behavior of TRTE

TRTEs can be strongly sorbed by Fe/Mn-oxides in slightly acidic percolation solutions (pHs < 6) (McKenzie, 1980; Marques et al., 2004). However, V was found to be insignificantly correlated with Fe_2O_3 ($r_{V\text{-}Fe}$ = −0.007, −0.012, −0.141) and Cr was weakly negatively correlated with Fe_2O_3 in all three profiles ($r_{Cr\text{-}Fe}$ = −0.460, −0.484, −0.174). Sc, Ni, and Co were likely incorporated into Fe/Mn-oxides, because they exhibited a positive relationship with Fe_2O_3 and Mn in the three profiles ($r_{Sc\text{-}Fe}$ = 0.544, 0.531, 0.141; $r_{Co\text{-}Fe}$ = 0.407, 0.116, 0.370; $r_{Co\text{-}Mn}$ = 0.820, 0.675, 0.314; $r_{Ni\text{-}Mn}$ = 0.722, 0.053, 0.420). In addition, Ni, Co, Cu, and Zn exhibited their mobilization and re-precipitation frequently co-associating with each other, because they had moderate to strong positive correlations with each other in profiles A and C ($r_{Co\text{-}Ni}$ = 0.806, 0.521; $r_{Co\text{-}Zn}$ = 0.793, 0.441; $r_{Ni\text{-}Cu}$ = 0.909, 0.672; $r_{Ni\text{-}Zn}$ = 0.868, 0.871; $r_{Cu\text{-}Zn}$ = 0.758, 0.822).

5.1.3. Behavior of HFSE

Nb and Ta displayed similar $\tau_{i,j}$ patterns due to similarity of chemical properties. The $\tau_{i,j}$ patterns of Zr and Hf were also similar, as they belong to group IVB. Zr is commonly found in quartz, and Zr tended to co-associate with SiO_2 in profiles A and C ($r_{Si\text{-}Zr}$ = 0.844, 0.799), and was negatively correlated with SiO_2 in profile B ($r_{Si\text{-}Zr}$ = −0.667). All HFSEs were significantly correlated (r > 0.80) and frequently co-associated with each other. Assuming that Ti is conservative (inert index), HFSE may have been enriched or removed from the three profiles, indicating that HFSEs were relatively mobile with mobility increasing with increasing weathering degree.

5.2. REE behavior and fractionation during weathering

Mobility differences among REEs observed during weathering likely resulted in REE fractionation in weathering profiles. The REE normalization results of profile A demonstrated the lack of significant weathering fractionation among LREEs and the relatively little impact on REE fractionation in the regolith and saprock zone (Fig. 5a). LREE accumulation increased with weathering degree and resulted in significant HREE depletion pattern. Meanwhile, MREE displayed a depletion pattern in the saprock zone and an enrichment pattern in the regolith zone in profile B and C (Fig. 5b and c). Therefore, chemical weathering processes appear to exert significant effect on REE fractionation at profiles B and C, in agreement with above results from the REE mobility analysis (Fig. 4). This observation is important given that REEs are generally found to be more mobile in profile C than in profile B, with the lowest mobility observed in profile A (Fig. 4a–i).

Quantitative expressions of REE fractionation typically use $(La/Yb)_N$ ratios, which indicate the degree of steepness or separation between LREE and HREE during weathering process (e.g., Aubert et al., 2001; Ji et al., 2004; Yusoff et al., 2013). Other approaches refine REE further by showing inter-group fractionations between LREE and MREE $(La/Sm)_N$ and between MREE and HREE $(Gd/Yb)_N$ (e.g., Ji et al., 2004; Stille et al., 2009). $(La/Yb)_N$, $(La/Sm)_N$, and $(Gd/Yb)_N$ ratios are provided in Table 2 and plotted in Fig. 8. In profile A (Fig. 8a), LREE/MREE and LREE/HREE fractionation occurred in the regolith zone, because $(La/Sm)_N$ and $(La/Yb)_N$ ratios of regolith were less than those of parent materials. However, significant REE fractionation occurred in the saprock, as shown by the high values of $(La/Sm)_N$ and $(Gd/Yb)_N$. In profile B (Fig. 8b), REE maintained uniform fractionation patterns. But, significant LREE/HREE fractionation occurred at 1.0 m, and LREE/MREE and MREE/HREE fractionation occurred at 3.2 m. These results are consistent with HREE enrichment and MREE depletion patterns, respectively (Fig. 5b). In profile C (Fig. 8c), the $(La/Yb)_N$ fractionation factor decreased with increasing depth, while $(La/Sm)_N$ and $(Gd/Yb)_N$ remained constant along transect, indicating significant LREE/HREE fractionation, which is consistent with the results of LREE enrichment analysis. These results suggest that LREE enrichment is a result of both LREE accumulation and depletion in HREE (Fig. 5c).

5.3. Factors controlling trace elements and REEs mobilization/fractionation

Mobilization and fractionation of trace and REEs in chemical weathering profiles are primarily constrained by weathering conditions (e.g., climate, solution pH, and solution complexes) and relevant primary and secondary minerals (e.g., goethite, titanite, and colloid) (Panahi et al., 2000; Ji et al., 2004; Feng, 2011; Ma et al., 2011a). Li et al. (2014) also demonstrated that biological processes are an important factor in dissolution of minerals; these processes may support differential recycling or differentiation of elements in profile A. Subtropical climate and different topographies likely caused the formation of three different weathering degree profiles, resulting in an increase in trace and REEs mobility with weathering degree.

In equilibrium with atmospheric CO_2 and O_2, meteoric water with dissolved carbon dioxide and dissolved oxygen (DO) can become weakly acidic and infiltrate into deep black shale. Pyrite and organic matter are oxidized by DO to produce sulfuric acid and organic acid in solution. The percolating solution decreases pH within the weathering profile and can lead to dissolution of primary minerals (e.g., albite, calcite, and apatite) and mobilization of trace and REEs coupled with primary minerals. The pH of the percolating solutions is an important factor that controls the mobilization and redistribution of the trace and REEs in the weathering profile. In this study, pH exhibited positive correlation with REE, especially MREE ($r_{MREE\text{-}pH}$ = 0.657, 0.556, 0.275; $r_{HREE\text{-}pH}$ = 0.496, 0.281, 0.388), and also with trace elements ($r_{Sr\text{-}pH}$ = 0.767, 0.564, 0.559). The leaching of trace and REEs is pH dependent; solubility of trace and REEs will

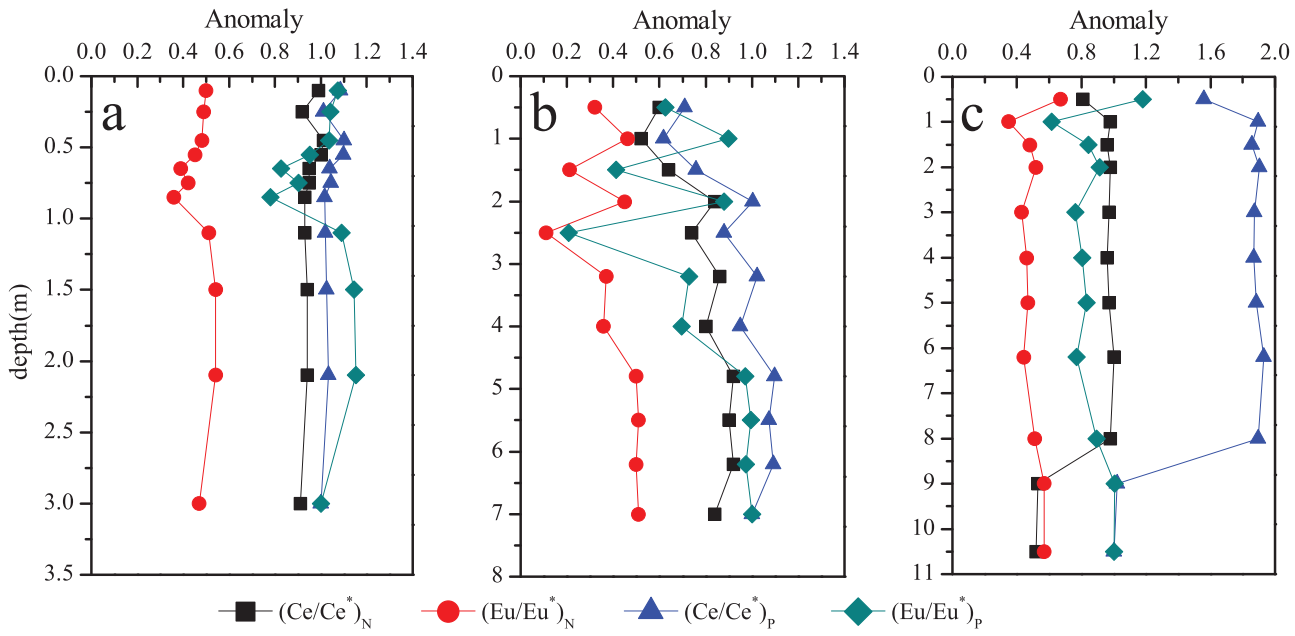

Fig. 8. The rations of $(La/Yb)_N$, $(La/Sm)_N$, and $(Gd/Yb)_N$ plotted with depth profiles in (a) profile A, (b) profile B, and (c) profile C at Chengkou County.

increase and MREE tends to dissolve more readily than HREE and LREE at low pH, while higher pH can induce precipitation (data and figure in Appendix Table 3 of Supplementary information; Duddy, 1980; Aubert et al., 2001; Patino et al., 2003; Sun et al., 2012). The percolating acidic solution can easily carry migrating REEs from the middle section of saprock zone at low pH into the bottom of the saprock zone and fractured shale (Table 2). The MREEs exhibited depletion pattern in the saprock zone in all three profiles, which is consistent with MREE dissolution and displayed enrichment in solution at lower pH from acidic water/shale interaction experiment (Appendix Table 3 of Supplementary information; Olías et al., 2005; Zhao et al., 2007; Ferreira da Silva et al., 2009). As the percolating solution interacts with shale at middle depths of profiles, H^+ ion concentrations decrease in the solution, resulting in an increase in the pH value. This phenomenon results in re-precipitation of trace elements and REEs as hydroxides and/or in the adsorption of these elements onto clay mineral surfaces. In addition, the depth of re-precipitation (saprock front) was found to increase with increasing weathering degree. This observation was consistent with the depth of the saprock front in profile C, which was greater than that in profiles A and B.

Primary minerals play an important role in mobilizing REE and trace elements. Previous studies have shown that muscovite, monazite, and apatite are particularly important factors in trace element and REE mobility (Compton et al., 2003; Yusoff et al., 2013). A significant positive correlation was found among MREE, HREE, and P_2O_5 ($r_{MREE\text{-}P}$ = 0.730, 0.475, 0.214; $r_{HREE\text{-}P}$ = 0.765, 0.569, 0.264). Ni, Nb, and Ta were mobilized as a result of apatite decomposition (Fig. 7a and c). These phenomena show that P-bearing minerals (e.g., apatite) play an important role in controlling trace and REEs mobilization during weathering. Eu^{2+}, Ca^{2+}, and Sr^{2+} possess identical chemical charge and similar ion radii. Therefore, Eu^{2+} can easily replace Ca^{2+} or Sr^{2+} in Ca- or Sr-bearing minerals in the weathering profile (Panahi et al., 2000), in agreement with the positive correlation with each other ($r_{Eu\text{-}Ca}$ = 0.457, 0.438, 0.405; $r_{Eu\text{-}Sr}$ = 0.494, 0.172, 0.598). Muscovite and albite also dominate the REE content during weathering processes. Thus, Muscovite, albite, and apatite are important factors in the evolution of fractionation patterns. As chemical weathering progresses, trace and REEs can also be gradually released from the breakdown of more resistant minerals (e.g., zircon, titanite) and can then be taken up by solutions, leading to mobility, enrichment/depletion, and fractionation within the profiles.

Aside from primary minerals, secondary minerals (colloids) and organic matters are also important factors affecting the mobilization and fractionation of trace elements and REEs (Stille et al., 1999; Aubert et al., 2001; Sun et al., 2012). As weathering proceeds, Fe, Al, and Mn were released from primary mineral and formed secondary minerals and colloids. Thus, Fe/Al/Mn- oxides or hydroxides may also result in elemental enrichment or depletion in weathering profiles (e.g., Pokrovsky and Schott, 2002; Neaman et al., 2005; Pokrovsky et al., 2010; Andrews et al., 2011), which is consistent with significant relationship among LREE, Al, and Mn in these three profiles ($r_{LREE\text{-}Al}$ = 0.514, 0.360, 0.485; $r_{LREE\text{-}Mn}$ = 0.604, 0.733). Some trace elements, such as TRTEs, can be sorbed by Fe/Mn-oxides during weathering process as discussed previously. Additionally, Pb element has affinity for Fe/Mn-phases as weathering proceeds in three profiles ($r_{Pb\text{-}Fe}$ = −0.023, 0.335, 0.499; $r_{Pb\text{-}Mn}$ = −0.301, 0.561, 0.418), indicating that Pb may be increasingly adsorbed in the secondary Fe/Mn- oxides or hydroxides with increasing weathering degree (Tuttle et al., 2009). Differences in the relative affinities of REE are ultimately caused by chemical property, which results in preferential scavenging of MREE and HREE and subsequent transport through the solution, but LREEs were strongly retained by clay minerals and colloids on the surface of silicate (Fig. 7b and d; Åström and Corin, 2003; Bao and Zhao, 2008). Organic matter can also form organic colloids or ligands (Andrews et al., 2011). Several trace elements are strongly sorbed by organic matters ($r_{OM\text{-}Sr}$ = 0.701, 0.317, 0.874; $r_{OM\text{-}U}$ = 0.792, 0.241, 0.763). MREEs and HREEs were also affected by organic matter in profile C, which was exposed to moderate to intense weathering ($r_{OM\text{-}MREE}$ = 0.604; $r_{OM\text{-}HREE}$ = 0.678). Together these processes resulted in LREE/MREE and HREE fractionation during chemical weathering.

6. Conclusion

The results of the present study suggest the following generalized conclusions:

(1) Based on mass transfer coefficient ($\tau_{i,j}$) calculations, Mn, Sr, Ba, Pb, U, V, Cr, Co, Ni, Cu, and Zn are easily mobilized in

weathering profiles, whereas Sc, Rb, and Th patterns are relatively immobile compared to Ti. The high field strength elements are also mobile during weathering, demonstrating Nb-Ta and Zr-Hf covariant mobilization. The depth of trace elements mobilization and re-precipitation (saprock front) increases with increasing weathering intensity.

(2) LREE, MREE, and HREE displayed similar behavior. All REE are enriched in the regolith zone in mid-ridge (A) and near mountaintop (B) profiles, while depleted in saprock zone in all three profiles. Preferential removal of MREEs relative to HREEs and LREEs at low-pH occurs in the saprock zone. REE mobilization ($\tau_{i,j}$ value) is dependent on pH and increases with weathering intensity. So this weathering leads to a fractionation so that depletion of MREE is stronger than that of HREE and LREE in saprock zone, resulting in LREE enrichment increase with increasing weathering degree. The REE fractionation sequence is as follows: valley (C) >near mountaintop (B) >mid-ridge (A). The positive Ce anomalies relative to parent shale result suggest the development of oxidizing conditions as weathering proceeds.

(3) Trace elements and REEs are retained in primary minerals and form certain secondary minerals; these elements are mobilized as primary minerals decompose. The behavior of trace elements and REEs during mobilization and redistribution differs when they are affected by pH value, weathering intensity, and secondary mineral phases, especially Fe/Al/Mn oxides or hydroxides. Therefore, solution pH, primary minerals, and secondary minerals play important roles in the mobilization, redistribution, and fractionation of trace and REEs in black shale weathering profiles.

Acknowledgements

We are most grateful to Shiming Wang and Jiewei Li for guidance with sample selection and field investigation. The authors thank the associated editor and two anonymous reviewers for their critical comments and constructive suggestions, which helped to improve the manuscript. This study was financially supported by research funds awarded by the National Natural Science Foundation of China (Nos.41172261, 41472256, 51348003), the Key Technology Research and Development Program of Sichuan Province, China (No. 2012SZ0051), Program for Excellent Innovation of PhD candidate in SWJTU (2015-40), and Project for Top-notch Innovation of Rail-transit Industry in SWJTU (2012-19).

Appendix A. Supplementary data

Supplementary data associated with this article can be found, in the online version, at http://dx.doi.org/10.1016/j.chemer.2015.07.004

References

Aiuppa, A., Allard, P., D'Alessandro, W., Michel, A., Parello, F., Treuil, M., Valenza, M., 2000. Mobility and fluxes of major, minor and trace metals during basalt weathering and groundwater transport at Mt. Etna volcano (Sicily). Geochim. Cosmochim. Acta 64, 1827–1841.

Alibo, D.S., Nozaki, Y., 1999. Rare earth elements in seawater: particle association, shale-normalization, and Ce oxidation. Gechim. Cosmochim. Acta 63 (3–4), 363–372.

Amundson, R., 2004. Soil formation. In: Holland, H.D., Turekian, K.K. (Eds.), Treatise on Geochemistry, 01. Elsevier Press, Amsterdam, pp. 1–35, Chapter 5.01.

Anderson, S.P., Dietrich, W.E., Brimhall, G.H., 2002. Weathering profiles, mass-blalance analysis, and rates of solute loss: linkage between weathering and ersion in a small, steep catchment. Geol. Sci. Am. Bull. 114, 1143–1158.

Andrews, D.M., Lin, H., Zhu, Q., Jin, L., Brantley, S.L., 2011. Hot spots and hot moments of dissolved organic carbon export and soil organic carbon storage in the Shale Hills Catchment. Vadose Zone J. 10, 943–954.

Anjum, F., Bhatti, H.N., Asgher, M., Shahid, M., 2010. Leaching of metal ions from black shale by organic acids produced by *Aspergillus niger*. Appl. Clay Sci. 47, 356–361.

Åström, M., Corin, N., 2003. Distribution of rare earth elements in anionic, cationic and particulate fractions in boreal humus-rich streams affected by acid sulphate soils. Water Res. 37, 273–280.

Aubert, D., Stilie, P., Probst, A., 2001. REE fractionation during granite weathering and removal by waters and suspended loads: Sr and Nd isotopic evidence. Geochim. Cosmochim. Acta 65 (3), 387–406.

Bao, Z., Zhao, Z., 2008. Geochemistry of mineralization with exchangeable REY in the weathering crusts of granitic rocks in South China. Ore Geol. Rev. 33, 519–535.

Bau, M., 1991. Rare-earth element mobility during hydrothermal and metamorphic fluid-rock interaction and the significance of the oxidation state of europium. Chem. Geol. 93, 219–230.

Beyala, V.K.K., Onana, V.L., Priso, E.N.E., Parisot, J.C., Ekodeck, G.E., 2009. Behaviour of REE and mass balance calculations in lateritic profile over chlorite schists in South Cameroon. Chem. Erde 69, 61–73.

Brantley, S.L., Godhaber, M.B., Ragnarsdottir, K.V., 2007. Crossing disciplines and scales to understand the critical zone. Elements 3, 307–314.

Braun, J.J., Pagel, M., Herbillon, A., Rosin, C., 1993. Mobilization and redistribution of REEs and thorium in a syenitic lateritic profile: a mass balance study. Geochim. Cosmochim. Acta 57, 4419–4434.

Braun, J.J., Ngoupayou, J.R.N., Viers, J., Dupre, B., Bedimo, J.P.B., Boeglin, J.L., Robain, H., Nyeck, B., Freydier, R., Nkamdjou, L.S., Rouiller, J., Muller, J.R., 2005. Present weathering rates in a humid tropical watershed: Nsimi, South Cameroon. Geochim. Cosmochim. Acta 69 (2), 357–387.

Brimhall, G.H., Dietrich, W.E., 1987. Constitutive mass balance relations between chemical composition, volume, density, porosity, and strain in metosomatic hydrochemical system: results on weathering and pedogenesis. Gechim. Cosmochim. Acta 51, 567–587.

Brimhall, G.H., Chadwick, O.A., Lewis, C.J., Compston, C.J., Williams, I.S., Danti, K.J., Dietrich, W.E., Power, M.E., Hendricks, M.E., Bratt, J., 1991. Deformational mass transport and invasive process in soil evolution. Science 255, 695–702.

Brookins, D.G., 1989. Aqueous geochemistry of rare earth elements. Rev. Mineral. Geochem. 21, 201–225.

Compton, J.S., White, R.A., Smith, M., 2003. Rare earth element behavior in soils and salt pan sediments of a semi-arid granitic terrain in the Western Cape, South Africa. Chem. Geol. 201, 239–255.

Duddy, I.R., 1980. Redistribution and fractionation of rare earth elements and other elements in a weathering profile. Chem. Geol. 30, 363–381.

Duff, M.C., Coughlin, J.U., Hunter, D.B., 2002. Uranium co-precipitation with iron oxide minerals. Geochim. Cosmochim. Acta 66, 3533–3547.

Faimon, J., 2003. Formation of colloidal silica and alumina during experimental granodiorite weathering. Aquat. Geochem. 9, 305–341.

Feng, J.L., 2010. Behaviour of rare earth elements and yttrium in ferromanganese concretions, gibbsite spots, and the surrounding terra rossa over dolomite during chemical weathering. Chem. Geol. 271, 112–132.

Feng, J.L., 2011. Trace elements in ferromanganese concretions, gibbsite spots, and the surrounding terra rossa overlying dolomite: their mobilization, redistribution and fractionation. J. Geochem. Explor. 108, 99–111.

Ferreira da Silva, E., Bobos, I., Xavier Matos, J., Patinha, C., Reis, A.P., Cardoso Fonseca, E., 2009. Mineralogy and geochemistry of trace metals and REE in volcanic massive sulfide host rocks, stream sediments, stream waters and acid mine drainage from the Lousal mine area (Iberian Pyrite Belt, Portugal). Appl. Geochem. 24, 383–401.

German, C.R., Holliday, B.P., Elderfield, H., 1991. Redox cycling of rare earth elements in the suboxic zone of the Black Sea. Geochim. Cosmochim. Acta 55, 3553–3558.

Gong, Q., Deng, J., Yang, L., Zhang, J., Wang, Q., Zhang, G., 2011. Behavior of major and trace elements during weathering of sericite-quartz schist. J. Asian Earth Sci. 42, 1–13.

Herndon, E.M., Jin, L., Brantley, S.L., 2011. Soils reveal widespread manganese enrichment from industrial inputs. Environ. Sci. Technol. 45, 241–247.

Jaffe, L.A., Peucker-Ehrenbrink, B., Petsch, S.T., 2002. Mobility of rhenium, platinum group elements and organic carbon during black shale weathering. Earth Planet. Sci. Lett. 198, 339–353.

Jenner, G.A., 1996. Trace element geochemistry of Ti, Y and Zr in Ascot Formation metabasalts, SE Quebec. Contrib. Mineral. Petrol. 75, 79–87.

Ji, H., Wang, S., Ouyang, Z., Zhang, S., Sun, C., Liu, X., Zhou, D., 2004. Geochemistry of red residua underlying dolomites in karst terrains of Yunnan-Guizhou Plateau: II. The mobility of rare earth elements during weathering. Chem. Geol. 203, 29–50.

Jin, L., Ravella, R., Ketchum, B., Bierman, P.R., Heaney, P., White, T., Brantley, S.L., 2010. Mineral weathering and elemental transport during hillslope evolution at the Susquehanna/shale Hills Critical Zone Observatory. Geochim. Cosmochim. Acta 74, 3669–3691.

Jin, L., Brantley, S.L., 2011. Soil chemistry and shale weathering on a hillslope influenced by convergent hydrologic flow regime at the Susquehanna/shale Hills Critical Zone Observatory. Appl. Geochem. 26, S51–S56.

Koppi, A.J., Edis, R., Field, D.J., Geering, H.R., Klessa, D.A., Cockayne, D.J.H., 1996. Rare earth element trends and cerium-uranium-manganese associations in weathered rock from Koongarra, Northern Territory, Australia. Geochim. Cosmochim. Acta 60 (10), 1695–1707.

Lee, J.S., Chon, H.T., Kim, K.W., 1998. Migration and dispersion of trace elements in the rock-soil-plant system in areas underlain by black shales and slates of the Okchon Zone, Korea. J. Geochem. Explor. 65, 61–78.

Li, J., Sun, W., Wang, S., Sun, Z., Ling, S., Peng, X., 2014. Bacteria diversity, distribution and insight into their role in S and Fe biogeochemical cycling during black shale weathering. Environ. Microbiol. 16 (11), 3533–3547.
Ling, S., Wu, X., Zhao, S., Liao, X., Ren, Y., Zhu, B., 2014. Geochemical mass balance and elemental transport during the weathering of the black shale of Shuijingtuo formation in Northeast Chongqing, China. Sci. World J. 2014, 742950.
Lipinski, M., Warning, B., Brumsack, H.J., 2003. Trace metal signatures of Jurassic/Cretaceous black shales from the Norwegian shelf and the Barents Sea. Palaeogeogr. Palaeoclimatol. Palaeoecol. 190, 459–475.
Liu, Y., Liu, H.C., Li, X.H., 1996. Simultaneous and precise determination of 40 trace elements in rock samples using ICP-MS (in Chinese with English abstract). Geochimica 25 (6), 552–558.
Ma, J.L., Wei, G.J., Xu, Y.G., Long, W.G., Sun, W.D., 2007. Mobilization and re-distribution of major and trace elements during extreme weathering of basalt in Hainan Island, South China. Geochim. Cosmochim. Acta 71, 3223–3237.
Ma, L., Jin, L., Brantley, S.L., 2011a. How mineralogy and slope aspect affect REE release and fractionation during shale weathering in the Susquehanna/Shale Hills Critical Zone Observatory. Chem. Geol. 290, 31–49.
Ma, L., Jin, L., Brantley, S.L., 2011b. Geochemical behaviors of different element groups during shale weathering at the Susquehanna/shale Hills Critical Zone Observatory. Appl. Geochem. 26, S89–S93.
MacRae, N.D., Nesbitt, H.W., Kronberg, B.I., 1992. Development of a positive Eu anomaly during diagenesis. Earth Planet. Sci. Lett. 109, 585–591.
Marques, J.J., Schulze, D.G., Curi, N., Mertzman, S.A., 2004. Trace element geochemistry in Brazilian Cerrado soils. Geoderma 121, 31–43.
McKenzie, R.M., 1980. The adsorption of lead and other heavy metals on oxides of manganese and iron. Aust. J. Soil Res. 18 (1), 61–73.
Middelburg, J.J., van der Weijden, C.H., Woittiez, J.R.W., 1988. Chemical processes affecting the mobility of major, minor and trace elements during weathering of granitic rocks. Chem. Geol. 68, 253–273.
Morgan, B., Rate, A.W., Burton, E.D., Smirk, M., 2012. Enrichment and fractionation of rare earth elements in FeS- and organic-rich estuarine sediments receiving acid sulfate soil drainage. Chem. Geol. 308–309, 60–73.
Moyes, L.N., Parkman, R.H., Charnock, D.J., Livens, F.T., Hughes, C.R., Braithwaite, A., 2000. Uranium uptake from aqueous solution by interaction with goethite, lepidocrocite, muscovite and mackinawite: an X-ray absorption spectroscopy study. Environ. Sci. Technol. 34, 1062–1068.
Ndjigui, P.D., Bilong, P., Bitom, D., Dia, A., 2008. Mobilization and redistribution of major and trace elements in two weathering profiles developed on serpentinites in the Lomié ultramafic complex, South-East Cameroon. J. Afr. Earth Sci. 50, 305–328.
Neaman, A., Chorover, J., Brantley, S.L., 2005. Element mobility patterns record organic ligands in soils on early earth. Geology 33 (2), 117–120.
Nesbitt, H.W., 1979. Mobility and fractionation of rare elements during weathering of a granodiorite. Nature 279, 206–210.
Nesbitt, H.W., Markovics, G., 1997. Weathering of granodioritic crust, long-term storage of elements in weathering profiles, and petrogenesis of siliciclastic sediments. Geochim. Cosmochim. Acta 61, 1653–1670.
Nguetnkam, J.P., Villiéras, F., Kamga, R., Ekodeck, G.E., Yvon, J., 2014. Mineralogy and geochemical behaviour during weathering of greenstone belt under tropical dry conditions in the extreme North Cameroon (Central Africa). Chem. Erde 74, 185–193.
Olías, M., Cerón, J.C., Fernández, I., De la Rosa, J., 2005. Distribution of rare earth elements in an alluvial aquifer affected by acid mine drainage: the Guadiamar aquifer (SW Spain). Environ. Pollut. 135, 53–64.
Panahi, A., Young, G.H., Rainbird, R.H., 2000. Behavior of major and trace elements (including REE) during Paleoproterozoic pedogenesis and diagenetic alteration of an Archean granite near Ville Marie, Quebec, Canada. Geochim. Cosmochim. Acta 64 (13), 2199–2220.
Patino, L.C., Velbel, M.A., Price, J.R., Wade, J.A., 2003. Trace element mobility during spheroidal weathering of basalts and andesites in Hawaii and Guatemala. Chem. Geol. 202, 343–363.
Peng, B., Song, Z., Tu, X., Xiao, M., Wu, F., Lv, H., 2004. Release of heavy metals during weathering of the lower Cambrian black shales in western Hunan, China. Environ. Geol. 45, 1137–1147.
Peng, B., Pietrzynski, A., Pieczonka, J., Xiao, M., Wang, Y., Xie, S., Tang, X., Yu, C., Song, Z., 2007. Mineralogical and geochemical constraints on environmental impacts from waste rock at Taojiang Mn-ore deposit, central Hunan, China. Environ. Geol. 52, 1277–1296.
Peng, B., Rate, A., Song, Z., Yu, C., Tang, X., Xie, S., Tu, X., Tan, C., 2014. Geochemistry of major and trace elements and Pb-Sr isotope of a weathering profile developed on the Lower Cambrian black shales in central Hunan, China. Appl. Geochem. 51, 191–203.
Piper, D.Z., Calvert, S.E., 2009. A marine biogeochemical perspective on black shale deposition. Earth Sci. Rev. 95, 63–96.
Pokrovsky, O.S., Schott, J., 2002. Iron colloids/organic matter associated transport of major and trace elements in small boreal rivers and their estuaries (NW Russia). Chem. Geol. 190, 141–179.
Pokrovsky, O.S., Viers, J., Shirokova, L.S., Shevchenko, V.P., Filipov, A.S., Dupré, B., 2010. Dissolved, suspended, and colloidal fluxes of organic carbon, major and trace elements in the Severnaya Dvina River and its tributary. Chem. Geol. 273, 136–149.
Sanematsu, K., Kon, Y., Imai, A., Watanabe, K., Watanabe, Y., 2013. Geochemical and mineralogical characteristics of ion-adsorption type REE mineralization in Phuket, Thailand. Miner. Deposita 48, 437–451.
Saunders, A.D., Tarney, J., Marsh, N.G., Wood, D.A., 1980. Ophiolites as ocean crust: a geochemical approach. In: Panayiotou, A. (Ed.), Ophiolites: Proceedings of the international Ophiolite Symposium, Cyprus, 1979. Ministry of Agriculture and Natural Resources. Geological Survey Department, Cyprus, pp. 193–204.
Schilling, J.G., 1973. Iceland mantle plume: geochemical study of reykjanes ridge. Nature 242, 565–571.
Sharma, A., Rajamani, V., 2000. Major element, REE, and other trace element behavior in amphibolite weathering under semiarid conditions in southern India. J. Geol. 108 (4), 487–496.
Sholkovitz, E.R., 1992. Chemical evolution of rare earth elements: fractionation between colloidal and solution phases of filtered river water. Earth Planet. Sci. Lett. 114, 77–84.
Sholkovitz, E.R., 1995. The aquatic chemistry of rare earth elements in rivers and estuaries. Aquat. Biochem. 1, 1–34.
Stille, P., Gauthier-Lafaye, F., Louvat, D., 1999. REE migration in groundwaters close to the natural fission reactor of Bangombé (Gabon): Sm-Nd isotope evidence. In Proceedings of the Oklo Phase II Workshop (eds. D. Louvat, V. Michaud and H. v. Maravic). EUR Report Series n 19,137, pp. 263-272, Brussels.
Stille, P., Pierret, M.C., Steinmann,M, Chabaux, F., Boutin, R., Aubert, D., Pourcelot, L., Morvan, G., 2009. Impact of atmospheric deposition, biogeochemical cycling and water-interaction on REE fractionation in acidic surface soils and soil water (the Strengbach case). Chem. Geol. 264, 173–186.
Sun, H., Zhao, F., Zhang, M., Li, J., 2012. Behavior of rare earth elements in acid coal mine drainage in Shanxi Province, China. Environ. Earth Sci. 67, 205–213.
Sun, S.S., McDonough, W.F., 1989. Chemical and isotopic systematic of oceanic basalts: implications for mantle composition and processes. Geological Society, London, Special Publication 42, 313-345.
Sverjensky, D.M., 1984. Europium redox equilibrium in aqueous solutions. Earth Planet. Sci. Lett. 67, 70–78.
Taylor, S.R., McLennan, S.M., 1995. The geochemical evolution of the continental crust. Rev. Geophys. 33 (2), 241–265.
Tuttle, M.L.W., Breit, G.N., Goldhaber, M.B., 2009. Weathering of the New Albany shale, Kentucky:. redistribution of minor and trace elements. Appl. Geochem. 24, 1565–1578.
van der Weijden, C.H., van der Weijden, R.D., 1995. Mobility of major, minor and some redox-sensitive trace elements and rare-earth elements during weathering of four granitoids in central Portugal. Chem. Geol. 125, 149–167.
Wu, X., Ling, S., Ren, Y., Liao, X., Zhao, S., Li, X., 2015. Elemental geochemistry and chemical weathering intensity of black shale in northeastern Chongqing Province. J. Earth Sci., in press (in Chinese with English abstract).
Yu, C., Peng, B., Peltola, P., Tang, X., Xie, S., 2012. Effect of weathering on abundance and release of potentially toxic elements in soils developed on lower Cambrian black shales, P.R. China. Environ. Geochem. Health 34, 375–390.
Yusoff, Z.M., Ngwenya, B.T., Parsons, I., 2013. Mobility and fractionation of REEs during deep weathering of geochemically contrasting granites in a tropical setting, Malaysia. Chem. Geol. 349–350, 71–86.
Zeng, J.H., Guo, K., Tian, K., Xu, T.W., 2012. Hydrodynamic evolution and hydrocarbon accumulation in the Dabashan Foreland Thrust Belt, China. Acta Geol. Sin. (English Edition) 86 (4), 912–923.
Zhao, F., Cong, Z., Sun, H., Ren, D., 2007. The geochemistry of rare earth elements (REE) in acid mine drainage from the Sitai coal mine, Shanxi Province, North China. Int. J. Coal Geol. 70, 184–192.